The United Nations University

GEOTHERMAL TRAINING PROGRAMME
Orkustofnun, Grensásvegur 9,
IS-108 Reykjavík, Iceland

Reports 1996
Number 18

A CONCEPTUAL RESERVOIR MODEL AND NUMERICAL SIMULATION STUDIES FOR THE MIRAVALLES GEOTHERMAL FIELD, COSTA RICA

Osvaldo E. Vallejos
Instituto Costarricense de Electricidad
Geothermal Development Office, Geothermal Resources Department
Miravalles Geothermal Field, Gayabo de Bagaces, Guanacaste,
COSTA RICA

ABSTRACT

Commercial exploitation of the Miravalles geothermal field started in 1994 with eleven production wells and six reinjection wells. In this report a general description of the field is given. A conceptual model is defined, based on estimated formation temperatures and initial pressures in twenty-five wells. In the conceptual reservoir model a 260°C upflow zone is proposed in the north and an outflow zone in the south. The geothermal fluid moves laterally to the south at -100 to -300 m a.s.l. The wellfield is clearly bounded to the west by cold temperatures and low pressures. The character of the eastern boundary is unknown due to a lack of data in that region. Lumped modelling simulation suggests that the Miravalles field will behave as a closed reservoir system for the next years, resulting in rapid drawdown with time. This model may be pessimistic as only net production is considered in the study. A 3-D natural state model simulates reasonably well the temperature distribution in the wellfield, by using a large recharge rate of 180 kg/s of 270°C fluid and very low thermal conductivity of model boundaries. Further modelling studies must address critical questions such as future development of a two-phase reservoir zone, the destiny of reinjected fluids and the nature of the outflow zone south of the wellfield.

1. INTRODUCTION

Geothermal exploration activities in Miravalles have been carried out since 1975. They led to the identification of a proven reservoir area of about 12 km^2, and a similar area is classified as a probable expansion sector. The proven area is actually under exploitation by a 60 MW$_e$ power plant and a 5 MW$_e$ modular plant. By late 1997 it is expected that operation of a 55 MW$_e$ unit will start and during 1998 a 27 MW$_e$ production unit will be added (ICE/ELC, 1995).

The Miravalles geothermal field is a typical high-temperature liquid-dominated reservoir. It is encountered at about 700 m depth, and reservoir temperatures are declining to the south and west. The estimated thickness of the reservoir is about 800-1000 m (ICE/ELC, 1995).

The thirty-nine wells drilled to date provide valuable information on subsurface conditions. In this report the downhole temperature and pressure surveys from twenty-five of these wells are used to evaluate the initial pressure and formation temperature distribution of the reservoir. A conceptual reservoir model is proposed. The response of the field to production is studied numerically by using two different approaches: 1) A lumped model for simulating only the pressure and the field's net production history, and 2) a 3-D numerical model which simulates the field's initial pressure and temperature distribution.

2. THE MIRAVALLES GEOTHERMAL FIELD

2.1 Location

The Miravalles geothermal field is located in the Guanacaste province, in the northwestern part of Costa Rica (Figure 1) to the south and southwest of the Miravalles. The field is located at a 150 km distance from San José, the capital of Costa Rica. This is about 225 km by car (ICE/ELC, 1995).

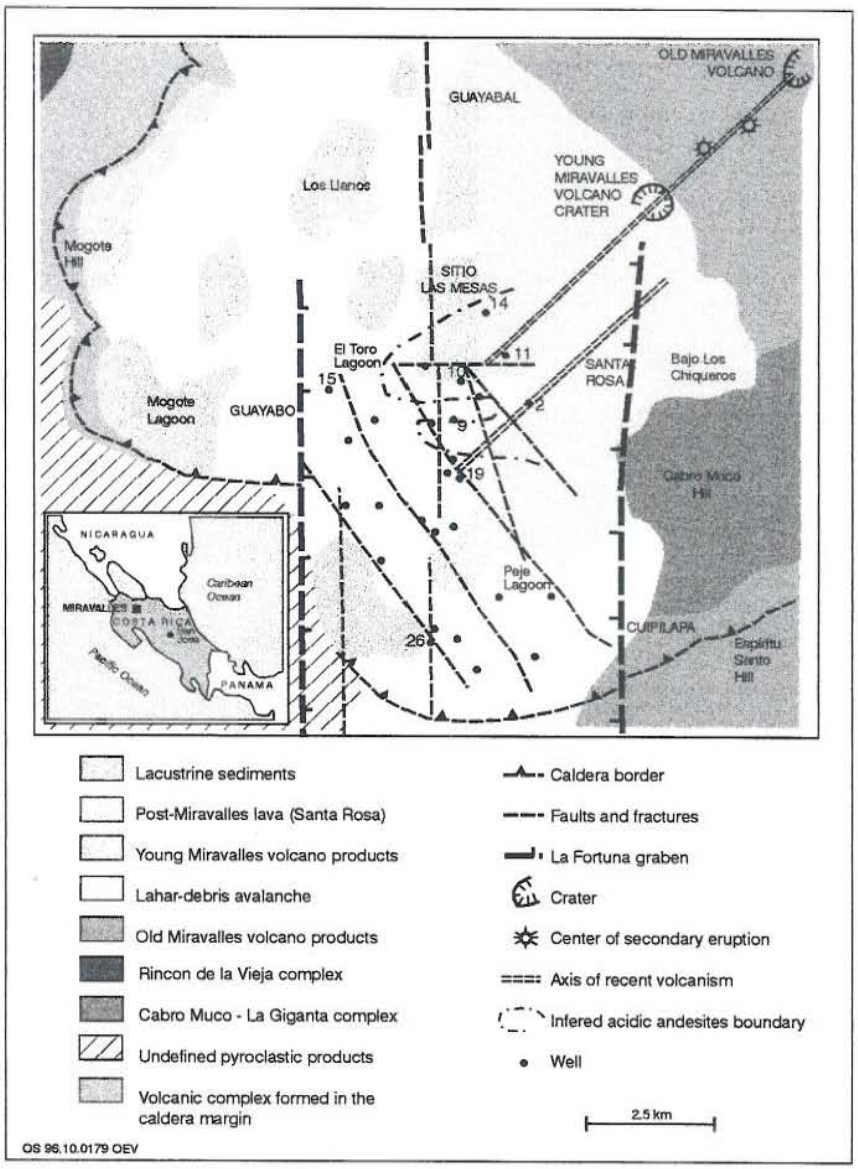

FIGURE 1: Location of the wells and geological structures in the Miravalles geothermal field

2.2 Geology

The Miravalles geothermal field is associated with a 15 km diameter wide caldera which has been affected by intense neo-tectonic phenomena. The interior of the caldera is characterized in general by a smooth morphology. The Miravalles volcano has an elevation of 2208 m a.s.l. This volcano is a part of the Guanacaste volcanic range. (ICE/ELC, 1995). The different lithostratigraphical units identified in the area from the deepest to the shallowest have been described by Herrera (1994) and the main features of the structural condition and alteration mineralogy of the area have been presented by ICE/ELC (1995).

2.2.1 Stratigraphy

The main stratigraphical units observed in Miravalles wells are as follows (Herrera, 1994):

Lava basement: It is characterized by porphyritic pyroxene-andesites formed before the calderic collapse.
Ignimbrite unit: It consists of welded tuff with abundant vitric matrix, polygenic lava and vitric fragments. Its emission promoted the caldera's sinking. Its thickness is about 1100 m (well PGM-15). It is located about -900 m a.s.l. and below.
Lava and tuff unit: It consists of an alternation of andesitic lavas with crystalline tuffs in a proportion of 2:1 with intercalation of arenaceous sediments and shale interbeds. It was formed by volcanic activity after the calderic collapse. It is some hundred meters thick in some parts of the field.
Volcano sedimentary unit: It consists of reworked crystalline and lithic tuffs with an interbedding of sandstones and shales of lacustrine origin. It has variable thickness from centimeters to tens of meters. The main part is located from -100 to -300 m a.s.l. Its thickness expands to about 800 m in the northeastern part.
Acid andesite unit: It consists of pyroxene-andesites characterized by common porphyritic-agglomerate texture, an above average porphyric index amphibole presence and a clinopyroxenes domain over the ortopyroxenes. The origin is attributed to the extrusion of intrusive bodies that formed dome structures in the surface and to the lava flow forming dome structures which occurred during the final deposition phase of the volcano sedimentary unit tuffs. It is found only in the northeastern part of the field. Its maximum thickness is 900 m (PGM-11).
Cabro Muco andesite unit: It consists of pyroxene-andesites with some occasional tuff intercalations. It is extended through the whole wellfield, except in the northwestern part, where it is replaced by the pumice unit (PGM-15), and in the southeastern part near well PGM-29 where it is not completely determined (very thin or replaced by a different unit). Its thickness is about 200-400 m, except in the south and southwest where it is only 60 m thick.
Pumice unit: It consists of pyroclastic products partly reworked and very rich in pumice. They come from relatively recent acid emissions. It is intersected in well PGM-15 and its thickness is about 300 m.
Post Cabro Muco volcanic unit: It consists of lahar and/or debris/avalanche alternations, andesitic lavas and basaltic andesites, lacustrine sediments and tuffs. They were derivated from the most recent volcanic activity mainly to the northeastern part of the field and also from landslides from the southern flank of the Miravalles edifice. The thickness of this unit is variable, from 300 m in the north east to 150 m in the meridional part of the field.

2.2.2 Structure

The field is located at the intersection of a caldera collapse and the La Fortuna graben complex. It is affected by recent intense tectonics originating from a difunded net of sub-vertical faults. The tectonics developed in different phases, with a preferential path originally in a NNW-SSE direction but presently

in a N-S direction. Maximum fracturing is observed in the central part of the caldera, but decreases to the west and east (ICE/ELC, 1995). The main features are as follows (Figure 1):

Caldera border: It corresponds to the Guayabo caldera limit. It is a morphological depression which is 15 km in diameter and sinking by about 200 m. The border is clearly recognizable in the west and northwest and partly in the south. In the northeast and east, the border has been covered with post-caldera volcanic products.
NNW-SSE fault system: This system was initially identified by geophysical prospecting and further confirmations have been found from well logs. These faults are hardly seen on the surface; in fact, the correlation between wells indicates that the surface displacements affect, in general, only the formations underlying the Post-Cabro Muco unit products, which show ancient tectonic activity without any important reactivation.
NE-SW axis of recent volcanism: The most recent eruptive centers which formed the Paleo-Miravalles (Old Miravalles) and Miravalles edifices are aligned over this axis. This axis corresponds to very deep faults which conducted magma to the surface. It is presumed that there are series of fractures with the same direction in the northeastern part of the field, which could be preferential paths for the rising of deep hot fluids to shallower parts.
Neo-tectonic N-S and W-E system: This system was the clearest surface evidence (river paths, hydrothermal manifestations, etc). The system is limited in the west and east by two N-S faults which define a 6 km high graben (La Fortuna graben). These faults exhibit a strong horizontal component. The graben is affected by intense faulting, which is manifested by N-S lineations of big lateral extension and W-E lineations concentrated in the northern part of the field.

2.2.3 Alteration mineralogy

Analysis of drill cuttings by X-ray diffractometric techniques have identified hydrothermal zones that reflect quite well the present thermal conditions with depth. The three main characteristic zones of identified clay minerals are as follows (ICE/ELC, 1995):

Smectite zone: Located between 400 and 600 m depth, it exhibits temperatures up to 150-180°C, and corresponds to the surface alteration processes and other deep hydrothermal processes which have affected the rock, forming the upper part of the reservoir caprock.
Transition zone: This is characterized by the smectite-illite interstratification, generally reaches 700-1000 m depth with temperatures of 160-220°C (with the highest alteration intensities), and includes the lower part of the reservoir caprock.
Illite zone: This characterizes the interior of the geothermal reservoir, with temperatures over 220°C. The alterations reflect mineralogical transformation and mineralogical deposition for a more direct hydrothermal flow supply. The depth to the top of this zone is variable.

2.3 Geochemistry

The reservoir fluids have a sodium-chloride composition with a TDS of 5300 ppm, a pH of 5.7 and a silica content of 430 ppm. In general, all the wells have similar chemical composition. There are, however, two wells with a very low pH and higher salinity fluids (PGM-02 and PGM-19). The noncondensible gas content in the steam, is in the range of 0.6 to 1.1% by weight. The reservoir fluid has a tendency to carbonatic scaling in the wells. The scaling is prevented by the injection of chemical inhibitors, but also by maintaining the wellhead pressure at over 6 bars. The reservoir fluids are noncorrosive. Good correlation is found between the Na/K, Na/K/Ca and Silica geothermometers and the downhole temperature data (ICE/ELC, 1995).

2.4 Hydrogeology

There are only a few thermal surface manifestations in the Miravalles field. These are related to neo-tectonic faults near well PGM-04. A hot spring area (around 60°C) discharges some water to the surface about 7 km south of the caldera border. A 600-700 m thick caprock otherwise blocks geothermal fluid flow to the surface. The main reservoir rocks are highly affected by hydrothermal alteration, mainly illite-epidote-titanite-chlorite-sericite associated with abundant quartz and calcite. This scaling tends to form a rigid rock mass, which is more sensible to fracturation. For that reason the reservoir permeability is assumed to be secondary. The landscape of the area permits a good meteoric recharge to the system (ICE/ELC, 1995).

There are three different permeable zones identified in the Miravalles field. The main zone is characterized by a lateral flow of 200-250°C temperature and a sodium-chloride composition. A shallow aquifer is located in the northeastern part of the field. It is located at about 200-250 m depth and it is a few tens of metres thick. It has variable permeability and is related to lacustrine sediments or some fractures. This aquifer is steam-dominated. It is formed by the evaporation of fluid from the main aquifer which moves along fractures. Finally, a deep acidic aquifer is located near wells PGM-02 (1700 m depth) and PGM-19 (960 m depth). It is not proven, however, that the acidic aquifer is the same in both locations (ICE/ELC, 1995).

2.5 Production history

The Miravalles geothermal field has been under commercial exploitation since March 25th of 1994, when 50 MW were generated by the first unit. Since then, 10 MW were added to the main unit, and 5 MW are generated by a modular unit. The total mass production is shown in Figure 2. It is obtained by correlating the wellhead pressures of the different wells with their respective output curves. Day 0 corresponds to March 25, 1994. The liquid-separated flow is mostly reinjected into the western and southern sectors of the well field, but the steam flow is used for electric generation. There are, however, some losses of the total mass produced from the field such as steam exhaust of the modular unit, the dragging of the cooling tower and some evaporation from the silica deposition pools.

Before the commissioning of the first unit, some mass extraction took place for well testing during an approximate five month testing period (power plant tests, pipelines cleaning and connections of the different wells with their respective separation units). The mass extraction in that period is estimated at 2 million tons (ICE/ELC, 1995). For the purposes of estimating the production history prior to the plant commissioning, this extraction is distributed as is shown in Figure 2 (period from -150 to 0 days). It takes into account the process followed during the test

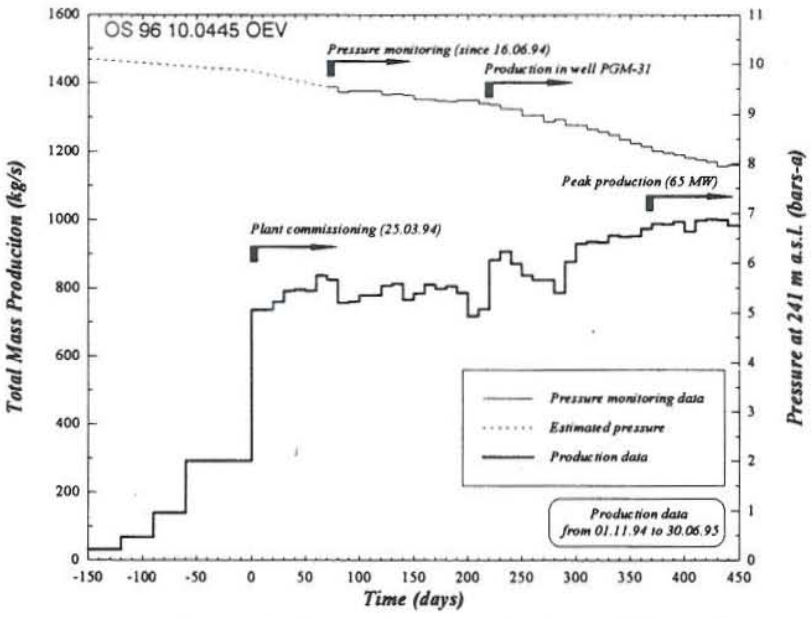

FIGURE 2: Production and pressure history of Miravalles (from November 1993 to June 1995)

period and the progressive connecting of the different wells to the steam gathering system.

Figure 2 also shows the pressure decline monitored in well PGM-09 from June, 1994 at 400 m depth (-241 m a.s.l.). Due to some delay in the bidding process, it was not possible to have the monitoring equipment available prior to the commissioning of the power plant. An initial reference pressure in well PGM-09 at the time of installation is also missing. In order to find this reference pressure and thus convert the collected pressure difference data in well PGM-09 to absolute pressure, the following approach is used:

1. The measured downhole pressure in well PGM-09 at -241 m a.s.l. in June 1994 was 9.55 bar-a. Taking this as the pressure condition in the well at the plant commissioning time gives a 70.8 bar-a at -500 m a.s.l. (ICE/ELC, 1995). Comparison with the pressure at the same depth in the 15.03.95 pressure survey gives a difference of about 0.8 bar between the two. Also observable in that survey is a pressure of 9.04 bar-a at -241 m a.s.l. Assuming that this pressure decline rate at -500 m a.s.l is valid for all the pressure history since the plant commissioning, it is possible to obtain a pressure of 9.84 bar-a at -241 m a.s.l. at time 0.

2. During the first 100 days of monitoring in well PGM-09, the pressure drop was about 0.0035 bar/day (ICE/ELC, 1995). Assuming that the pressure in well PGM-09 fell at that rate since the commissioning of the power plant (March 25, 1994), gives a cumulative pressure drop of 0.32 bars. Adding this pressure drop to the pressure monitored in well PGM-09 in June 1994, provides an initial pressure estimate 9.87 bars-a. This is near to the pressure estimate above.

3. Some pressure drop occurred in well PGM-09 during the time prior to plant commissioning (around 150 days). The initial pressure at -500 m a.s.l. in well PGM-31 (at 320 m distance of PGM-09) was 72 bar-a with 0.9 bars standard deviation (ICE/ELC, 1995). Taking the 06.02.93 pressure survey in well PGM-31 as a reference, the pressure at -500 m a.s.l. was 72.47 bar-a. The pressure at 241 m a.s.l. in the same survey was 10.71 bar-a. Correcting for the initial pressure, the pressure in well PGM-09 at day -150 may be 10.24 bar-a (10.71-0.47=10.24).

4. The mass extraction was almost doubled when the 55 MW started to produce commercially. Assuming that the pressure drop also doubled for that reason, the pressure drop during the 5 month testing period was only 1.75x10-3 bar/day. This means a cumulative pressure drop of 0.26 bar. Adding that pressure drop to the initial pressure estimate for time 0 (9.86 bar-a), the initial pressure in well PGM-09 was 10.12 bar-a, close to the initial pressure in well PGM-31.

In this report the undisturbed pressure in well PGM-09 at -241 m a.s.l. is, therefore, set at 10.1 bar-a. This pressure is important for the lumped modelling as will be seen later in this report.

3. EVALUATION OF THE MIRAVALLES GEOTHERMAL RESERVOIR

3.1 General information on the wells

Deep drilling in Miravalles started in 1979 with three exploratory wells, which proved the existence of a geothermal reservoir. After that, five more wells were drilled over a period from 1984 to 1986. Based on the downhole and production data, a 55 MW power generation appeared to be feasible for thirty years, with or without the reinjection of the separated geothermal brine (Haukwa et al., 1992). Due to some problems in the bidding processes, drilling was delayed until 1992 and is in continuous development by now. The location of the wells is shows in Figure 3, and Table 1 presents general information about them. Table 2 shows finally some information on the production characteristics of the wells used in this report.

TABLE 1: An overview of wells in the Miravalles geothermal field

Well	Drill date		Location		Well design		Depth (m)	Elevation (m a.s.l.)	Status
	From	To	N-S (m)	E-W (m)	End of casing (m)	End of liner (m)			
PGM-01	Mar.79	Jul.79	298995	406549	877	1295	1300	668	P
PGM-02	Nov.79	Oct.84	298846	407409	759	1988	2000	739	I
PGM-03	Jan.80	Mar.80	297584	405960	631	1029	1162	605	P
PGM-04	Aug.93	Nov.93	295997	404722	788	1799	2185	436	I
PGM-05	Feb.84	May.84	299514	405520	552	1837	1854	586	P
PGM-5R	Mar.85	Mar.85	299550	405497	181	255	272	586	S
PGM-08	Feb.94	Apr.94	298547	405664	764	1094	1200	610	S
PGM-09	Aug.93	Nov.93	298643	406062	766	1945	2001	641	M
PGM-10	May.84	Aug.84	299284	406235	725	1792	1797	654	P
PGM-11	Nov.84	Feb.85	299780	407149	797	1304	1455	719	P
PGM-12	Jun.85	Sep.85	296478	405679	544	1590	1597	517	P
PGM-14	Nov.93	Jan.94	300581	406793	892	1390	1396	703	S
PGM-15	Sep.85	Aug.92	299153	403744	956	2971	3022	559	N
PGM-16	Jun.92	Sep.92	294705	405770	838	1770	1799	446	I
PGM-17	Apr.93	Jul.93	297854	406078	744	1257	1300	624	P
PGM-19	Jun.93	Aug.93	297501	406225	806	1255	1260	609	D
PGM-20	Jan.93	Mar.93	296688	405492	783	1691	1700	517	P
PGM-21	Dec.92	Jun.93	296653	406045	887	1691	1716	529	P
PGM-22	Aug.92	Oct.92	298628	404623	876	1416	1427	578	I
PGM-23	Oct.94	Feb.95	298250	404127	958	---	2281	538	N
PGM-24	Oct.92	Dec.92	297017	404669	844	1958	1966	476	I
PGM-25	Jun.94	Oct.94	297062	404036	802	2254	2541	456	S
PGM-26	Apr.93	Jun.93	294412	405614	610	1515	1579	440	I
PGM-27	Jan.94	Feb.94	294507	406041	600	1558	1565	449	I
PGM-28	Feb.94	Apr.94	295185	406942	845	1309	1315	454	S
PGM-29	Jun.94	Jul.94	295296	407915	611	1375	1388	473	S
PGM-31	Oct.92	Jan.93	298909	406252	849	1171	1726	463	P
PGM-42	Aug.95	Nov.95	298908	405360	809	1576	1695	602	P
PGM-43	Oct.94	Dec.94	297881	405045	692	---	954	577	D
PGM-45	Dec.94	Mar.95	297750	405350	602	956	959	593	S
PGM-46	Dec.93	Jan.94	297366	405704	685	1187	1198	584	S
PGM-47	Apr.94	Jun.94	297099	405790	796	1503	1956	556	M
PGM-49	Apr.94	May.94	297051	405403	696	1304	1309	535	S
PGM-50	Mar.95	Aug.95	294012	407748	810	1497	1835	462	N-D
PGM-51	Jun.95	Sep.95	293828	405884	936	1373	1680	442	S
PGM-52	Mar.95	Jun.95	293822	406599	379	658	2367	436	S
PGM-56	Sep.95	Nov.95	294249	405760	736	816	819	438	S
PGM-58	Nov.95	Mar.95	300968	406963	807	1391	2443	728	M
PGM-59	Mar.96	Jun.96	294885	407873	851	1026	1026	457	S

Notes:
P: producing; I: injecting; S:stand-by; M: monitoring; N: non-productive; D: damaged.
(Data taken from ELC/ICE, 1995 and Engineering information sheets, ICE)

TABLE 2: Production characteristics of Miravalles wells (ICE/ELC, 1995)

Well	Feed zones (Depth in m and contribution in %)			Injectivity index (l/s/bar)	Productivity index (kg/s/bar)	Transmis-sivity (Dm)
PGM-01	850-900 (100)	---	---	NA	10.2	15-32
PGM-02	1000-1100 (30)	1600-1700 (70)	---	2.5	NA	7-18
PGM-03	700-800 (100)	---	---	NA	11.3	NA
PGM-04	1486-1500 (?)	>1778 (?)	---	3.8-5.2	NA	NA
PGM-05	1500-1650 (100)	---	---	0.9	2.1	29-82
PGM-08	784 (90)	1200 (10)	---	>15	>15	NA
PGM-09	1000	---	---	0.7	NA	NA
PGM-10	750 (50)	1250-1450 (50)	---	1.1	0.67	24-66
PGM-11	850-1000 (10)	1440 (90)	---	4-6	2.7-4.9	12-24
PGM-12	650-750 (?)	1000 (?)	1600 (?)	10	14-16	34.5
PGM-14	1125 (?)	>1396 (?)	---	10-13	NA	NA
PGM-15	?	---	---	0.7	NA	3
PGM-16	900-1100 (50)	1425 (33)	1550-1700 (17)	7.5-9	9.7	15
PGM-17	770-840 (?)	950-1000 (?)	1200-1500 (?)	11-14	10.4	NA
PGM-20	830 (?)	1320 (?)	1620 (?)	13	NA	NA
PGM-21	1000-1100 (90)	1450-1550 (10)	---	18	13.5	NA
PGM-22	1320 (100)	---	---	11-14	NA	NA
PGM-24	1020-1050 (70)	1790-1860 (30)	---	14	NA	NA
PGM-25	1075-1175 (?)	2000-2175 (?)	---	6-9	NA	NA
PGM-26	635 (90)	885 (10)	---	4	NA	NA
PGM-27	1470-1480 (100)	---	---	5-5.9	4.4	NA
PGM-28	1130-1240 (100)	---	---	>15	NA	NA
PGM-29	720 (15)	>1200 (85)	---	>20	NA	NA
PGM-31	850-1000 (30)	1400-1600 (70)	---	7.5-8.5	NA	NA
PGM-46	700 (67)	750-1198 (15)	>1186 (18)	>15	>15	NA

Notes: NA: not available

3.2 Evaluation of formation temperatures and initial pressures in the wells

The formation temperature of a well at different depths can be estimated during drilling by measuring the temperature recovery for some time at several depths. Once the data has been collected it is possible to apply some empirical methods which provide a prediction about the formation temperature. Among these methods are the Horner plot method and the Albright method (Helgason, 1993). Those methods can also be used for analysing well static temperature surveys, when temperature recovery data are not available. However, it is not always possible to apply those methods because boiling in the well or fluid flow through different zones might hide the true formation temperature. When this situation occurs it is necessary to analyse carefully the static temperature surveys and check them for one or two-phase conditions in comparison with the boiling point with depth curve. The initial pressure can finally be obtained by analysing the static pressure at different times.

Most of the wells in the Miravalles field were drilled between 1992 and 1995. As electric generation started in 1994, there are often only a few static logs available in the majority of the wells. The collected downhole data, together with the estimated formation temperature and initial pressure profiles, are shown in the next paragraphs. Finally, in Table 3 the initial pressure and formation temperature data are listed at selected depths.

WELL PGM-01 was the first of the three deep wells drilled in the early stages of Miravalles assessment. The estimated formation temperature mainly follows the survey from 19.02.81, except for some corrections in the zone between 500-800 m depth zone (Figure 4). From the surface to 350 m depth there are no data available, so in this zone the temperature is estimated, taking into account the existence of a shallow aquifer in the reservoir located at 200 m depth and using 25°C as the surface temperature (ICE, personal communication). Initial pressure estimate follows the survey of 15.07.80 (Figure 4).

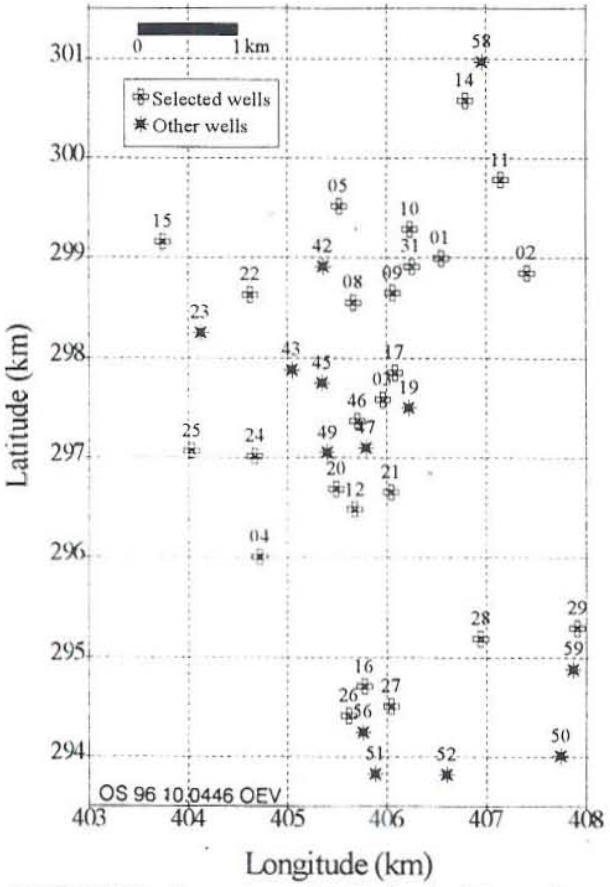

FIGURE 3: Location of wells in the Miravalles geothermal field

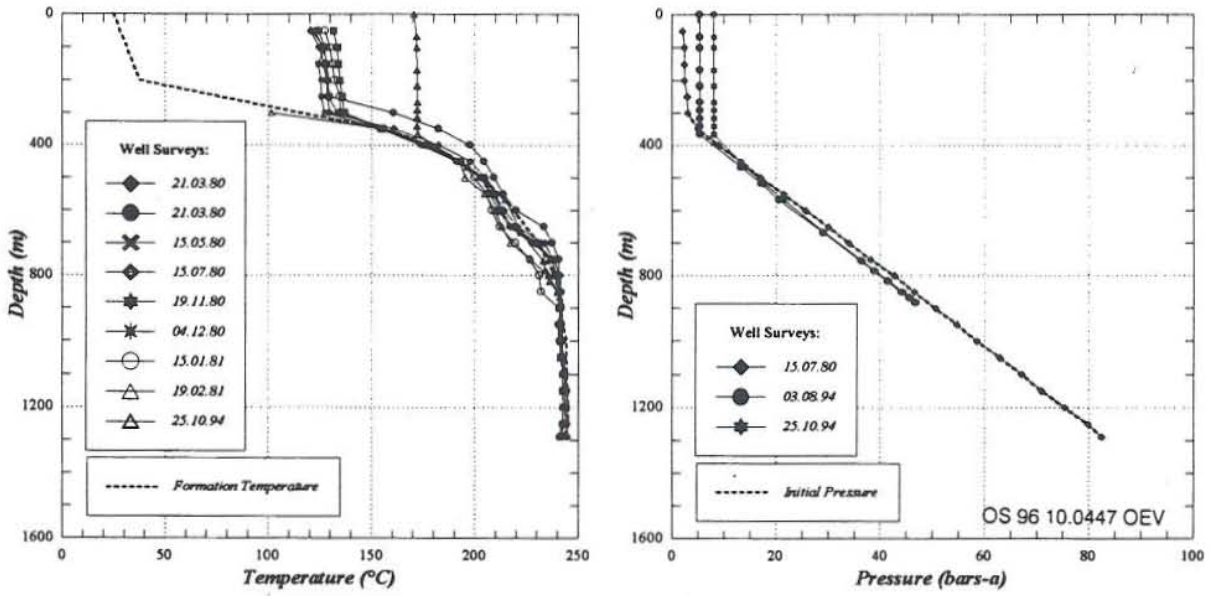

FIGURE 4: Formation temperature and initial pressure for well PGM-01

WELL PGM-02 was drilled in 1979 and deepened in 1984. During its deepening in 1984, an acid aquifer (pH of 2) was encountered at 1600 m depth. This well presents down-flow conditions (Figure 5). The estimated formation temperature and initial pressure are based on the surveys carried out on

TABLE 3: Formation temperature and initial pressure data for the Miravalles wells

Name	Temperature (°C) at selected depth (m a.s.l.)																						
	700	600	500	400	300	200	100	0	-100	-200	-300	-400	-500	-600	-700	-800	-900	-1000	-1100	-1200	-1300	-1400	-1500
PGM-01		29.30	35.60	89.99	164.04	196.52	214.85	226.80	236.12	240.61	243.35	244.49	244.98	244.40									
PGM-02	27.46	33.83	47.54	112.18	169.59	202.71	217.47	224.54	228.03	229.42	229.14	228.21	227.41	227.03	227.24	227.76	228.68	229.59	230.50	231.42			
PGM-03		25.70	33.72	73.17	112.03	151.16	188.33	226.63	236.83	239.07	239.07	239.07	239.07	239.07									
PGM-04				29.56	42.22	97.79	134.58	162.15	184.23	197.83	207.66	207.83	205.77	200.00	197.62	195.23	192.85	190.56	189.43	188.33	188.09	187.65	186.86
PGM-05			30.43	45.39	156.68	187.99	209.25	223.57	227.02	228.63	229.81	230.79	231.52	233.48	234.88	236.61	237.96	238.23	237.34	235.83	234.43	233.01	
PGM-08		21.57	38.60	93.33	122.85	152.01	175.47	202.17	224.31	237.38	234.94	233.14	233.95	234.89									
PGM-09		33.72	62.79	103.74	134.20	165.27	189.80	212.38	226.95	234.94	236.67	238.47	238.64	237.04	235.90	235.21	234.02	233.54	232.63	232.21	233.21		
PGM-10		28.31	34.68	90.69	170.67	202.08	222.70	238.17	248.19	248.45	247.47	246.33	245.12	240.16	239.72	239.39	238.92	237.83	236.83	235.95	235.31		
PGM-11	24.90	34.90	54.55	115.32	167.63	194.50	218.07	232.50	242.83	251.22	254.39	246.64	241.58	238.71	236.68	234.65	232.61						
PGM-12			26.49	35.82	84.28	122.43	160.59	198.74	213.46	221.73	226.34	227.97	229.38	230.26	230.61	231.05	231.39	231.32	231.32				
PGM-14	22.33	32.33	43.10	76.35	109.60	142.85	175.82	200.59	218.46	231.70	234.87	236.75	237.16	237.16	237.16	237.16	237.16						
PGM-15			29.50	30.44	36.25	51.80	64.70	75.08	86.06	98.30	112.33	123.42	134.50	145.58	155.33	163.10	169.44	175.80	182.16	187.84	193.04	198.24	203.37
PGM-16				29.93	52.51	104.17	157.03	209.89	221.17	228.22	232.44	232.85	232.51	232.18	231.77	231.27	230.42	229.17	227.93	228.16	230.24	233.49	236.74
PGM-17		27.68	29.63	94.74	149.23	184.76	204.86	221.18	230.34	235.79	237.80	238.37	238.82	238.68	235.59	232.49	229.39	226.29					
PGM-20			27.00	37.86	72.91	107.95	143.00	176.33	201.29	224.46	236.18	236.76	231.55	226.22	221.62	220.57	220.62	221.18	221.27	222.04	222.81	223.58	224.35
PGM-21			25.92	38.13	73.16	114.49	144.72	177.50	202.76	217.52	225.12	228.28	229.11	229.15	229.15	229.15	229.15	229.15	229.15	229.52	230.49	231.45	232.42
PGM-22			29.75	34.77	45.42	65.56	86.07	109.00	131.18	152.87	171.42	189.08	206.25	220.92	230.59	230.40	228.96	227.76					
PGM-24				33.47	66.11	112.72	166.36	195.55	203.34	211.12	218.91	223.96	226.84	227.18	226.75	226.64	226.52	226.41	226.06	225.75	225.03	222.88	220.32
PGM-25				32.15	46.10	57.70	69.30	79.10	90.07	101.03	112.00	138.40	157.10	185.90	193.10	198.30	198.50	200.10	198.10	198.20			
PGM-26				28.60	79.60	124.77	153.00	176.68	190.05	194.58	192.94	193.65	196.22	201.32	205.86	209.95	212.80	215.34	217.10	218.85			
PGM-27				26.76	42.56	78.36	125.63	170.70	199.74	212.22	220.62	223.46	222.83	220.50	218.16	215.82	213.49	211.15	211.84	220.22			
PGM-28				30.53	34.81	74.54	108.71	146.18	184.87	211.06	221.17	225.26	225.93	226.14	224.87	224.26	224.26	224.26	224.26				
PGM-29				31.32	33.96	71.28	108.61	145.93	194.12	226.53	229.46	229.74	230.05	229.86	230.20	230.57	230.80	231.67	232.54				
PGM-31		27.74	34.11	61.22	109.44	142.12	172.89	202.23	221.95	238.31	242.59	242.43	241.56	240.59	238.60	235.69	226.86	224.92	225.65	226.27	226.89	227.51	
PGM-46			31.74	65.35	98.76	134.29	169.00	205.03	232.48	237.30	237.16	237.20	237.35	237.39									

Name	Pressure (bars-a) at selected depth (m a.s.l.)																						
	700	600	500	400	300	200	100	0	-100	-200	-300	-400	-500	-600	-700	-800	-900	-1000	-1100	-1200	-1300	-1400	-1500
PGM-01				2.91	6.3	14.51	22.94	31.47	39.74	47.98	56.02	64.38	72.47	80.92									
PGM-02				3.26	9.47	17.38	25.61	33.86	42.12	50.27	58.46	66.62	74.81	82.7	90.18								
PGM-03					4.62	13.72	22.39	31.01	39.29														
PGM-04						6.51	15.09	23.59	31.91	40.34	48.85	57.24	65.56	73.92	82.32	90.83	99.53	108.2	116.7	125.35	134.08	142.95	151.75
PGM-05				4.39	7.48	16.11	24.07	32.38	40.32	48.5	56.44	64.31	72.18	80.55	88.75	96.87	104.97	113.13	121.37	129.57	137.75	145.95	
PGM-08				1.15	3.37	11.93	20.29	28.47	36.6	45.27	53.37	61.6	69.7	77.8									
PGM-09					5.24	13.48	21.66	29.71	38.26	46.79	54.68	62.79	71.03	78.93	86.89	94.83	103.15	110.9	118.97	126.89	135.2		
PGM-10				4.46	9.49	17.48	25.35	33.78	41.88	49.91	57.82	65.67	73.76	81.72	89.78	97.97	106.07	114.25	122.56	130.77	139.05		
PGM-11				5.29	9.91	17.95	26.15	34.32	42.29	50.24	58.12	66.03	73.91	81.81	89.72	97.63	105.53						
PGM-12					3.09	11.3	19.4	27.37	35.24	43.49	51.82	60.06	68.29	76.41	84.39	92.61	100.71	108.74	116.82				
PGM-14					1.29	10.21	18.65	26.65	35.44	44.97	53.19	61.26	69.26	77.89	86.5	95.1	103.71						
PGM-15					1	7.07	14.7	23.83	32.99	42.35	51.57	60.57	69.64	78.43	87.03	95.78	104.57	113.17	121.86	130.85	139.27	147.72	156.55
PGM-16					3.55	13.01	21.32	28.21	36.64	45.21	53.56	61.78	70.19	78.43	86.85	95.29	103.52	111.89	120.23	128.52	136.97		
PGM-17					4.04	12.12	20.35	28.51	36.46	44.5	52.63	60.95	68.93	77.32	85.09	92.95	100.81	108.67					
PGM-20					3.5	11.76	20.01	28.27	36.55	44.83	53.23	61.36	69.4	77.51	85.63	93.76	101.89	110.12	118.34	126.44	134.58	142.72	150.86
PGM-21					4	12.41	20.89	29.18	37.73	45.83	53.93	62.15	70.41	78.66	86.74	95.53	103.78	112.13	120.67	129.25	137.83	146.4	154.98
PGM-22					4.07	7.17	15.52	23.89	32.45	41.25	50.19	59.04	67.96	76.66	85.6	94.24	102.94	111.62					
PGM-24					2.2	12.14	21.53	30.61	39.7	48.38	57.05	64.99	72.72	81.53	90.71	0	107.31	115.61	123.87	131.94	140.22	148.47	156.73
PGM-25						4.77	12.87	21.95	31.13	40.37	49.74	58.97	67.89	76.74	85.5	94.23	103.08	111.92	120.74	129.62	138.49	147.29	156.16
PGM-26					4	11.98	20.18	28.78	37.64	46.45	55.41	64.13	72.91	81.74	90.56	99.31	107.96	116.58	125.22	133.86			
PGM-27					4.04	11.16	20.66	29.37	37.87	46.1	54.37	62.7	70.96	79.06	87.52	95.88	104.25	112.33	120.72	129.16			
PGM-28						9.12	18.06	27.05	35.38	43.8	52.71	61.07	69.42	77.58	85.82	93.88	101.97	110.04	118.12				
PGM-29					1.23	9.89	18.5	27.08	35.33	44.25	52.67	60.97	69.19	77.36	85.36	93.46	101.68	110	118.33				
PGM-31				2.11	5.65	14.36	23.23	31.78	39.96	47.99	56.07	64.39	72.39	80.4	88.41	96.49	105.03	112.88	120.96	129.12	137.28	145.44	
PGM-46					3.32	11.8	20.15	28.51	36.68	44.78	52.83	60.98	69.16	77.15									

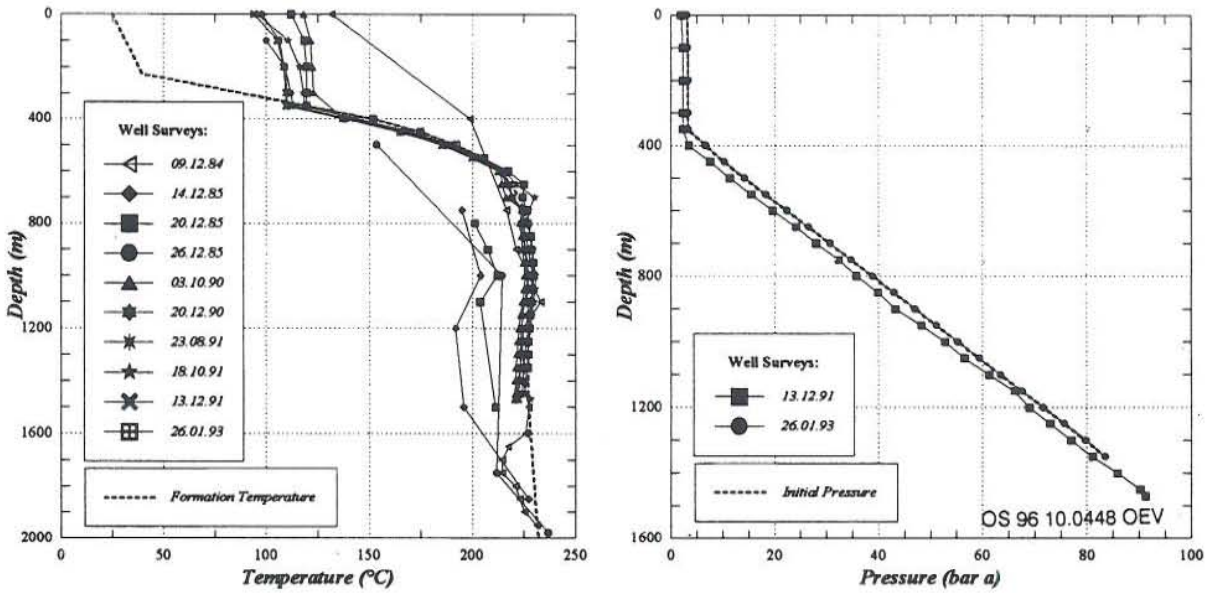

FIGURE 5: Formation temperature and initial pressure for well PGM-02

26.01.93. The formation temperature also takes into account a survey, made on 09.12.84, in the deepest part of the well. A temperature reversal is not considered for the static profile (Figure 5).

WELL PGM-03 was the third exploration well in Miravalles. This well has an obstruction initially at 580 m depth, but presently at 690 m depth. For this reason there is only one complete static survey available in the well. The estimated formation temperature is based on the 26.02.93 survey with some changes down to 700 m depth; from this point to the bottom hole, the formation temperature is based on the 17.02.81 survey. The estimated initial pressure is based on the 28/01/85 survey (Figure 6).

WELL PGM-04 has a total depth of 2185 m, but the liner ran to 1799 m due to the loss of some drilling equipment in the well. This well is used for reinjection of brine. The estimated formation temperature

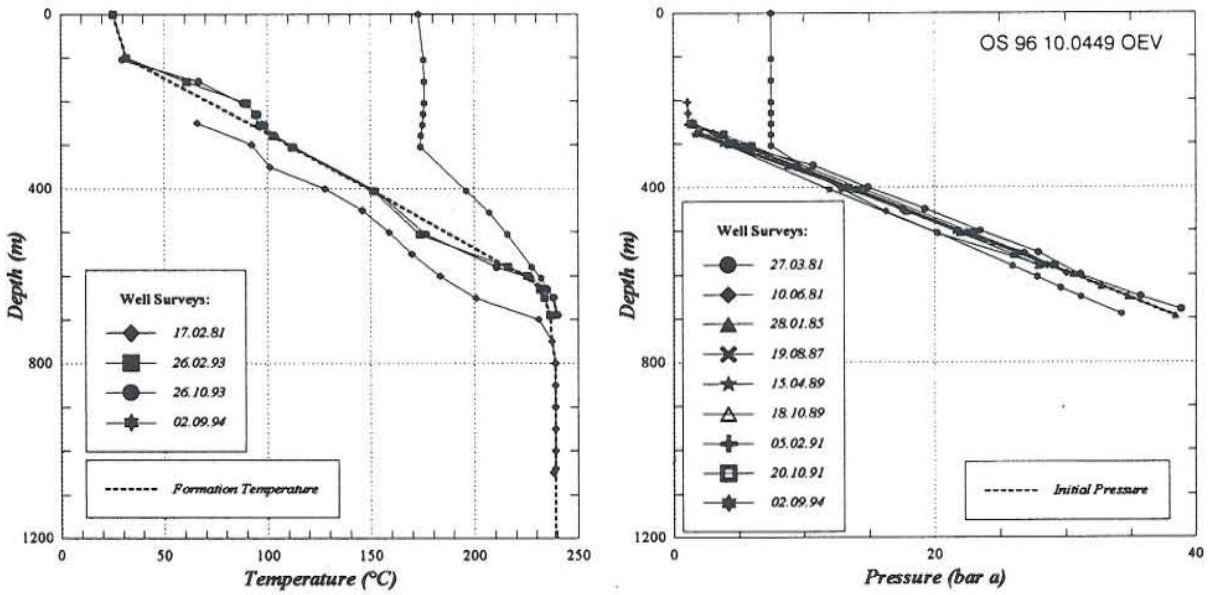

FIGURE 6: Formation temperature and initial pressure for well PGM-03

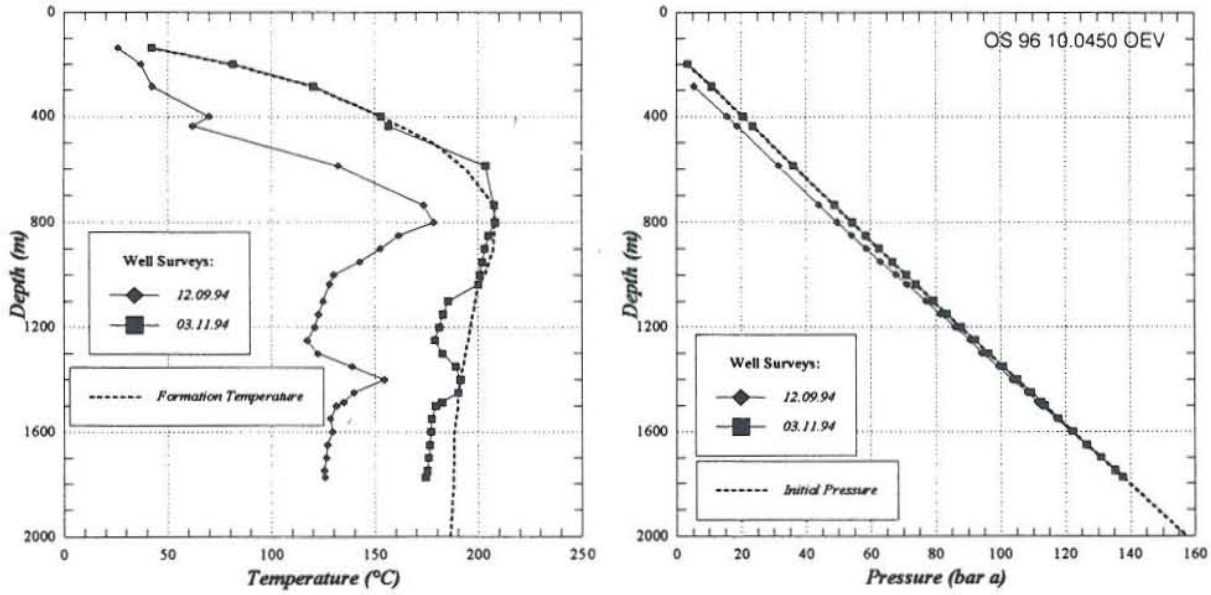

FIGURE 7: Formation temperature and initial pressure for well PGM-04

is based on the static survey of 03.11.94. It is possible that this well is hotter than the temperature measured. The estimated initial pressure is based on the 12.09.94 survey. The presence of a deep pivot point is clear in the pressure surveys, indicating that the deeper feed zone is the most productive one (Figure 7).

WELL PGM-05 has a maximum liner depth of 1837 m, but can only be logged down to 1825 m. The estimated formation temperature and initial pressure follow directly the 17.12.92 surveys (Figure 8).

WELL PGM-08 was drilled for the second power plant unit. The estimated formation temperature and initial pressure are based on the 26.11.94 surveys (Figure 9).

WELL PGM-09 was drilled as a production well for the second power plant unit, but due to poor productivity it was an unsuccessful well. The well is used for pressure monitoring. The 23.02.94 and

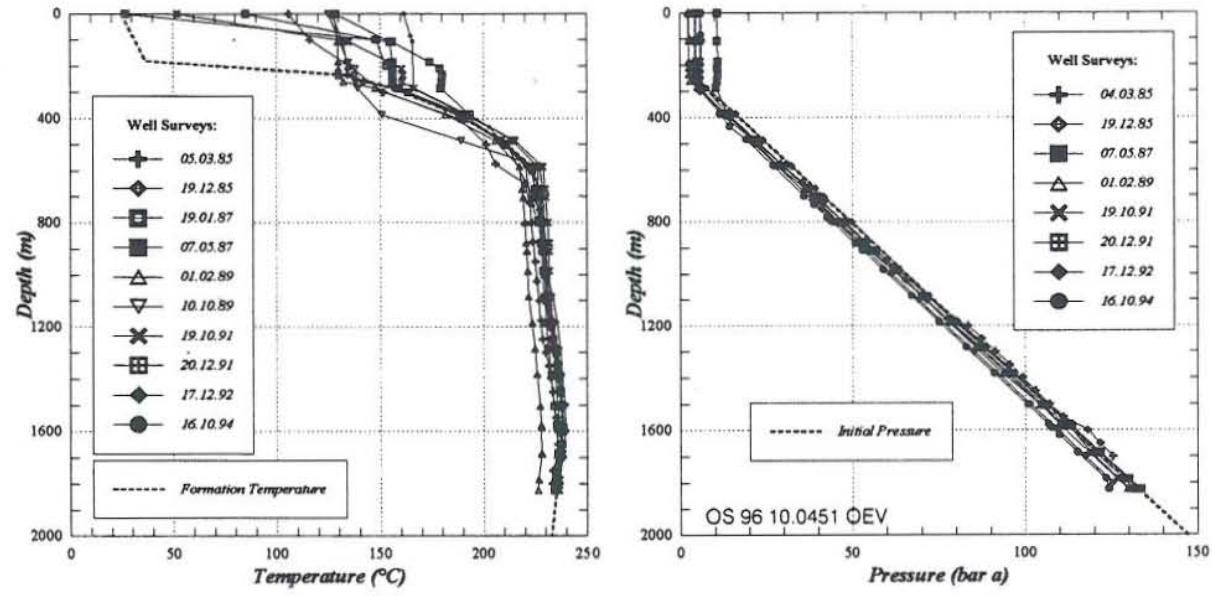

FIGURE 8: Formation temperature and initial pressure for well PGM-05

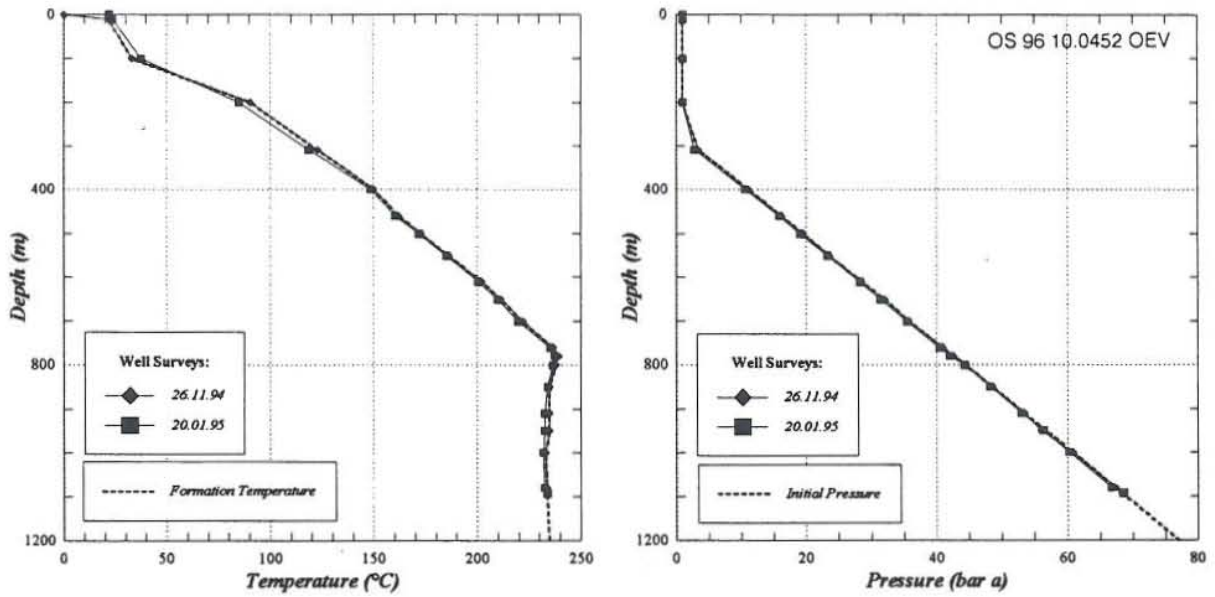

FIGURE 9: Formation temperature and initial pressure for well PGM-08

15.03.95 surveys are used for estimating the formation temperature, the first to 800 m depth, and the second one for the rest of the well (Figure 10). The temperature behaviour from 800 m to the bottom hole is considered correct because the well does not have a down-flow condition. The temperature reversal at the hole's bottom is due to drilling. The 15.03.95 survey is used as a reference for the initial pressure estimation. A pressure drawdown of about 1 bar had already taken place in the field at this time (Chapter 2.5). The initial pressure estimate is, therefore, raised by 1 bar from the 15.03.95 values.

WELL PGM-10 has a down-flow condition. The 26.01.93 survey is used as a reference for the estimated formation temperature. The temperature reversal is considered true. The initial pressure is assumed to follow the 18.01.93 survey (Figure 11).

WELL PGM-11 presents the highest temperature measured in the field (above 250°C). The well is in

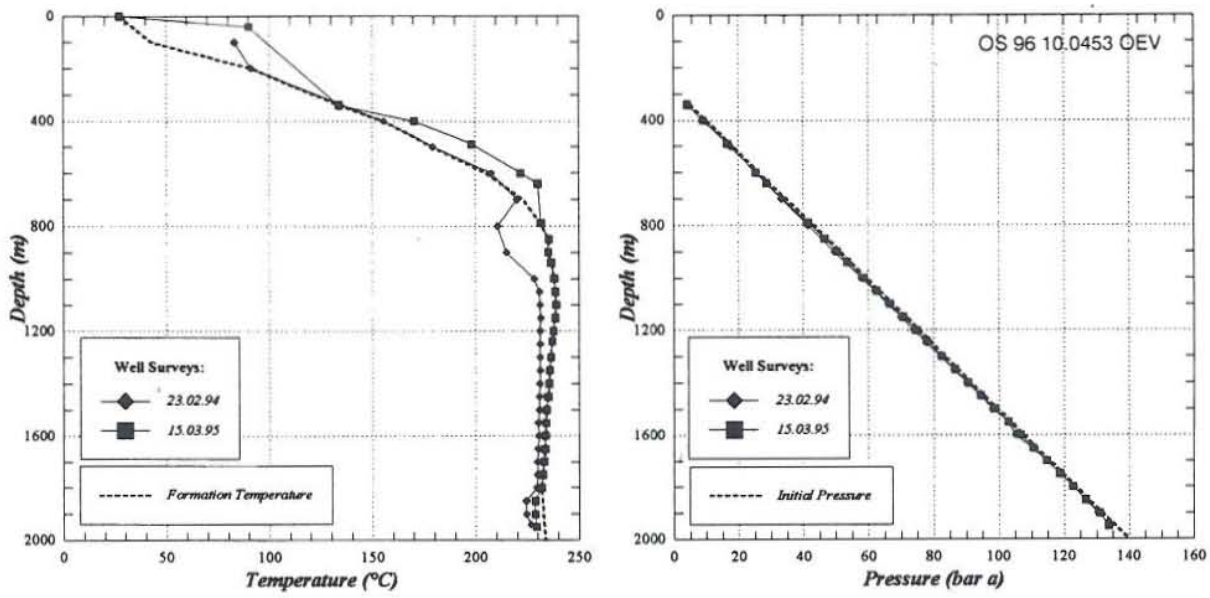

FIGURE 10: Formation temperature and initial pressure for well PGM-09

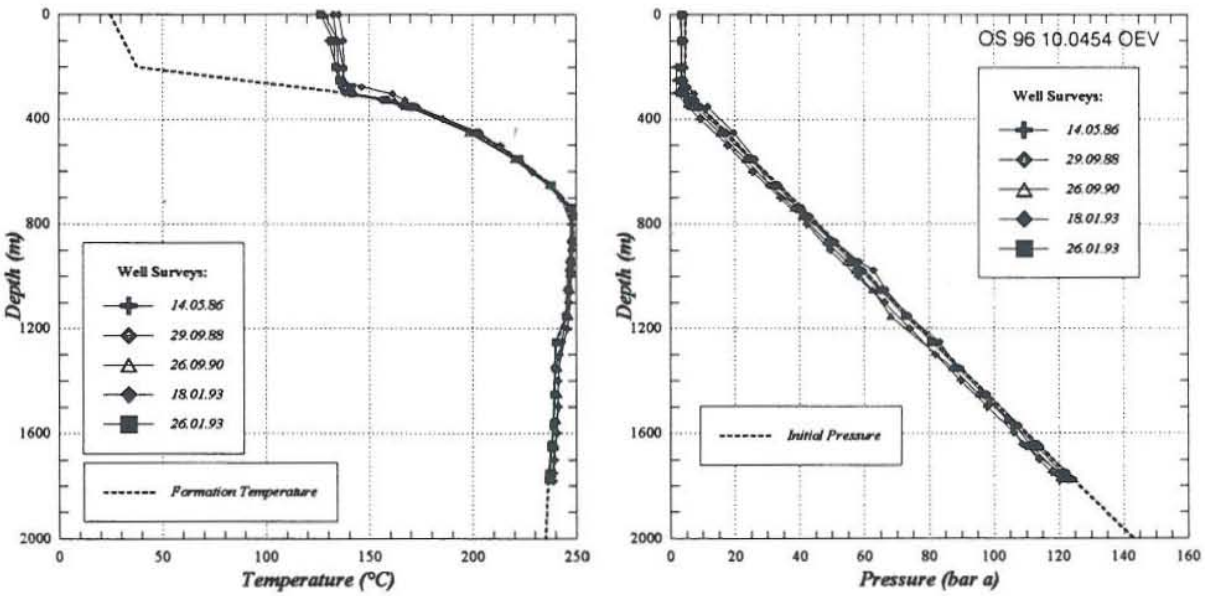

FIGURE 11: Formation temperature and initial pressure for well PGM-10

a down-flow condition. The surface temperature is taken from the 30.10.94 survey, and the estimated formation temperature is based on the 16.12.92 survey. The temperature reversal at the bottom of the hole is extended to 1600 m depth. The initial pressure is based on the 16.12.92 survey (Figure 12).

WELL PGM-12 had a serious casing damage, which was to be repaired by placing a less diameter casing to 405 m. Due to this situation and a cold water inflow, production was considerably decreased by calcite deposition in the liner. It was cleaned but never returned to its initial status. The estimated formation temperature is based on the 11.01.88 survey, including the shallow aquifer effect as is shown in the 22.10.93 survey. The initial pressure follows the 15.08.94 survey (Figure 13).

WELL PGM-14 was drilled as an exploration well for checking the area extent of the field. It is the

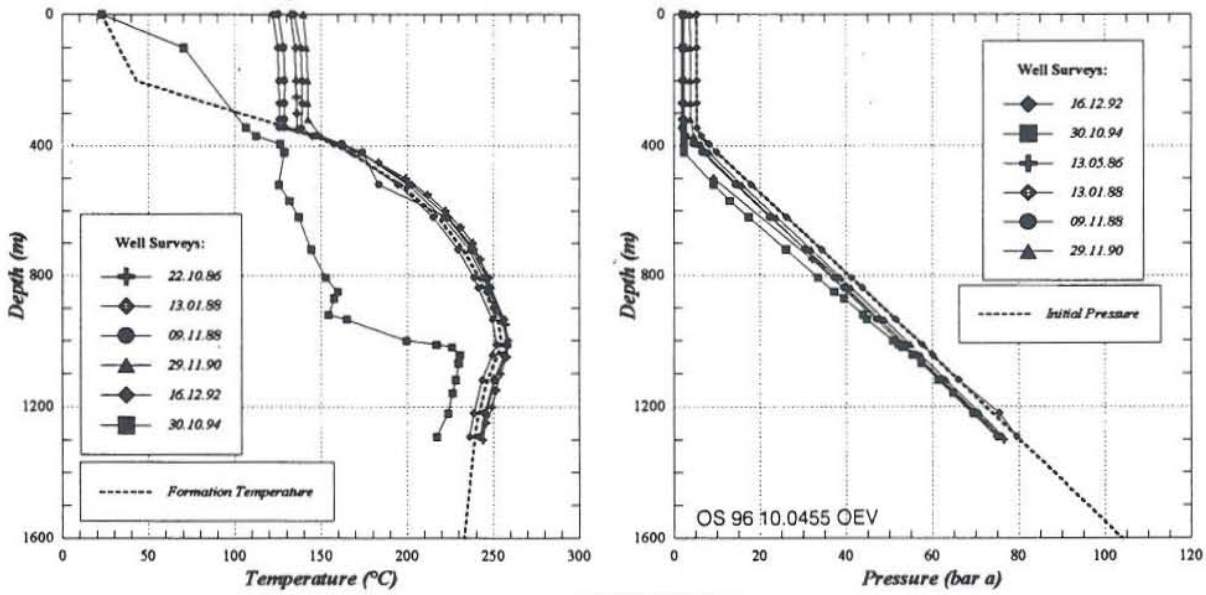

FIGURE 12: Formation temperature and initial pressure for well PGM-11

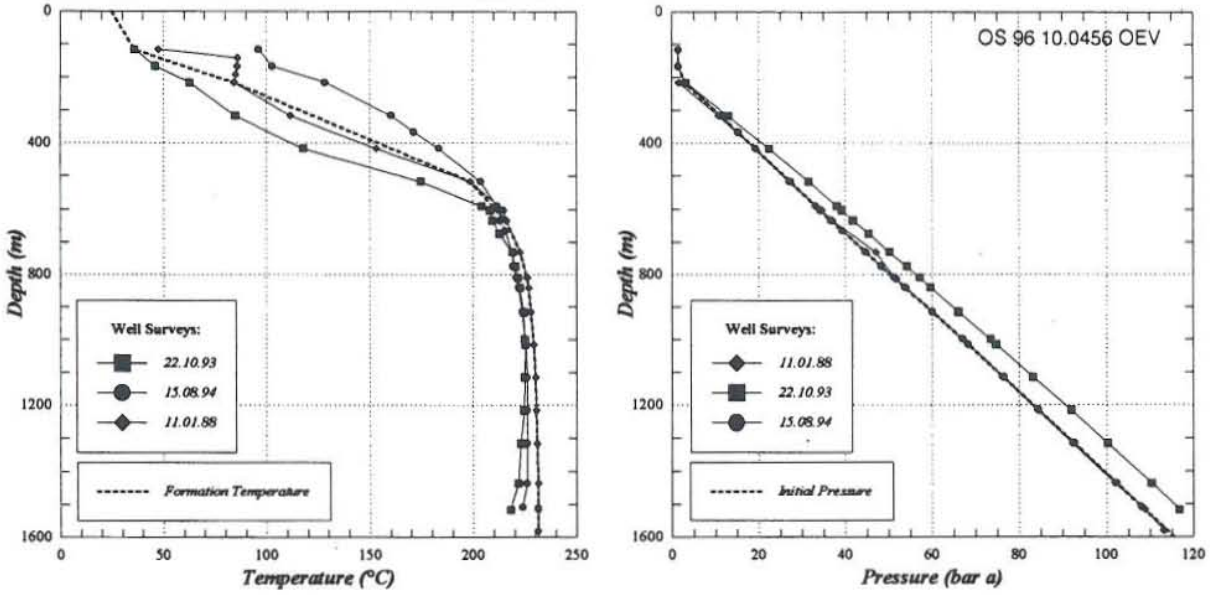

FIGURE 13: Formation temperature and initial pressure for well PGM-12

well located furthest northeast in Miravalles. It will be connected to the third unit. The estimated formation temperature follows the 07.04.95 survey, but is slightly corrected in the zone from the surface to 800 m. The temperature reversal observed in two of the surveys is due to casing repair operations. The initial pressure estimate is based on the 07.04.95 survey (Figure 14).

WELL PGM-15 is the deepest well in Miravalles and is totally unproductive. It is considered to define the field boundary. The estimated formation temperature follows the 13.10.94 survey with some corrections at 800-1200 m and 1300-1700 m, due to some internal circulation of fluid in the well. The initial pressure guess follows the 25.01.95 survey (Figure 15).

WELL PGM-16 was drilled as a reinjection well. This well presents down-flow conditions. The

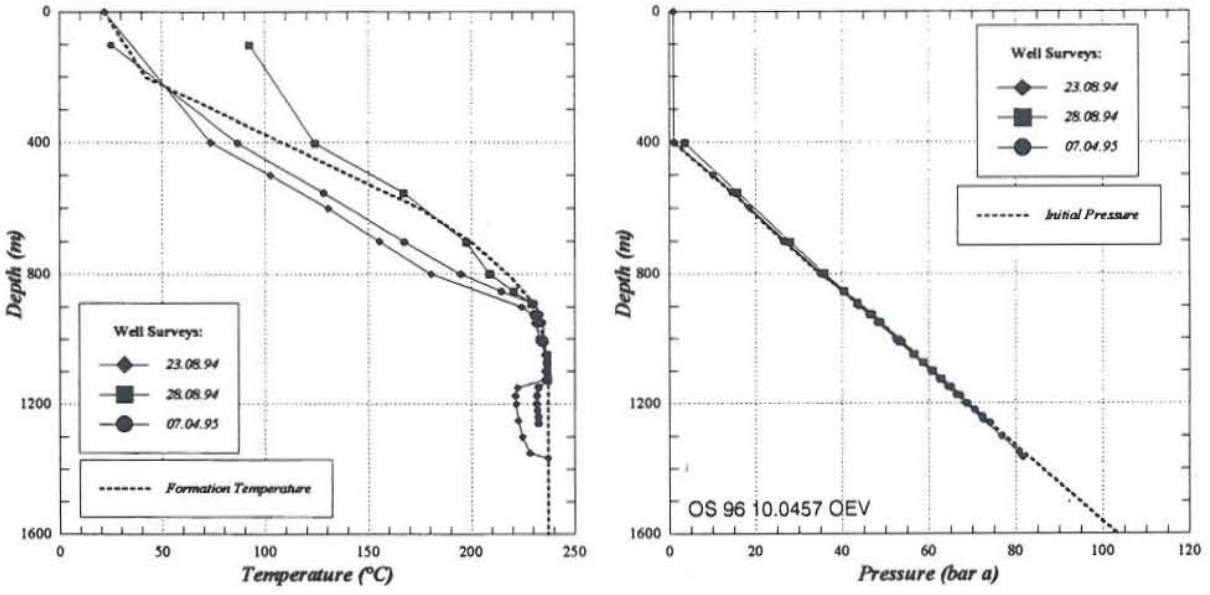

FIGURE 14: Formation temperature and initial pressure for well PGM-14

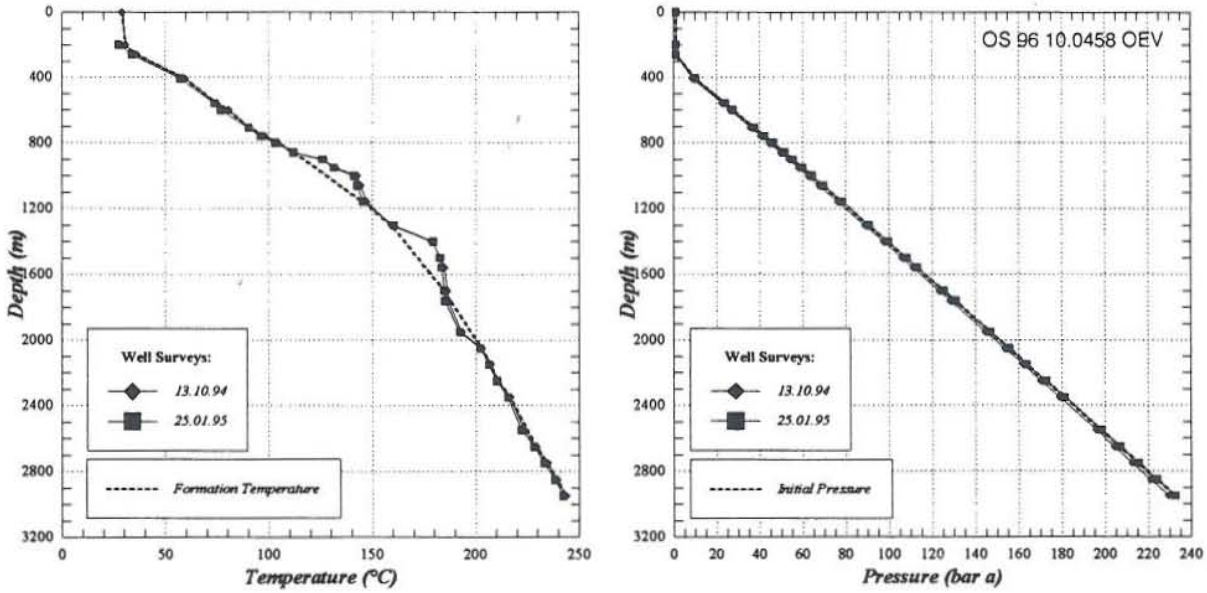

FIGURE 15: Formation temperature and initial pressure for well PGM-15

formation temperature is a combination of the 11.02.93 and the 24.11.95 surveys. A slight temperature reversal is proposed on the basis of the most recent profile, which is affected by reinjection. The 11.02.93 survey is used for estimating the initial pressure (Figure 16).

WELL PGM-17 shows down-flow conditions. The 18.12.94 survey is taken as the formation temperature profile, and the suggested temperature reversal is considered true. The initial pressure follows the 18.12.94 survey (Figure 17).

WELL PGM-20 presents down-flow conditions. The formation temperature is based on the 10.06.94 and 19.08.94 surveys. The first survey is assumed to be affected by down-flow and a temperature reversal is estimated from 850 m depth to the bottom hole. The 10.06.94 survey is used to estimate the initial pressure (Figure 18).

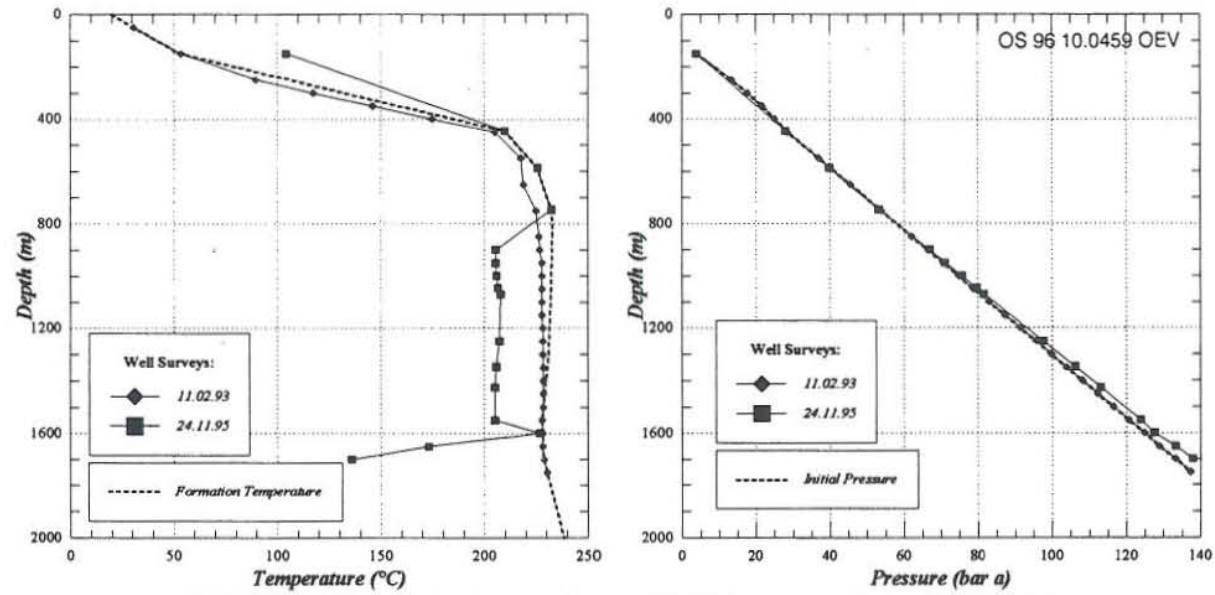

FIGURE 16: Formation temperature and initial pressure for well PGM-16

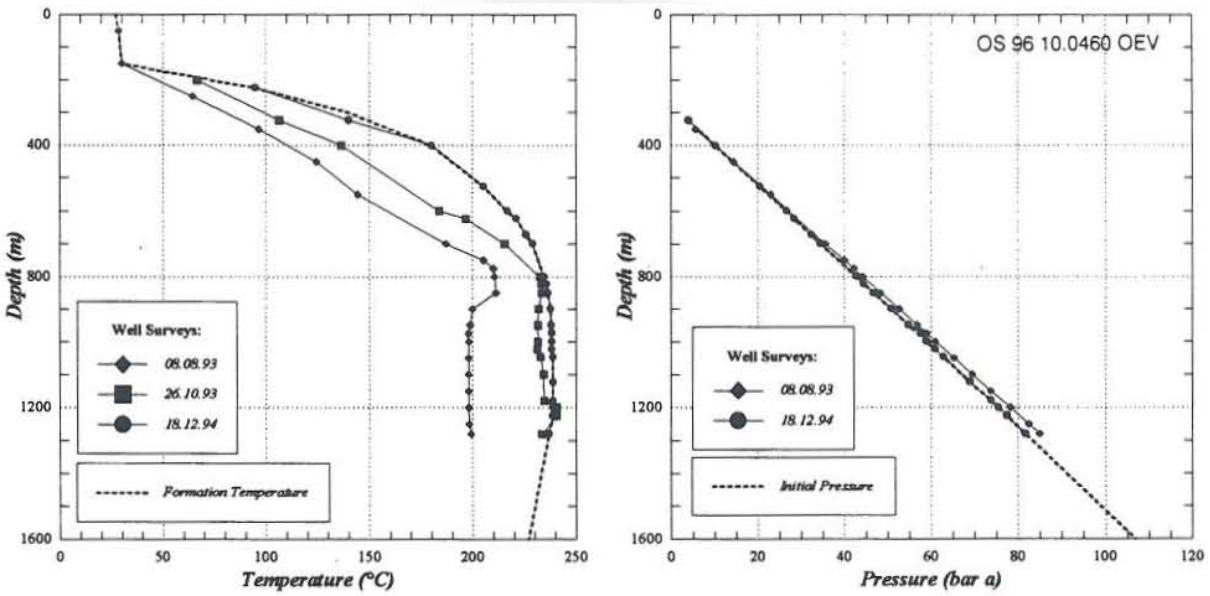

FIGURE 17: Formation temperature and initial pressure for well PGM-17

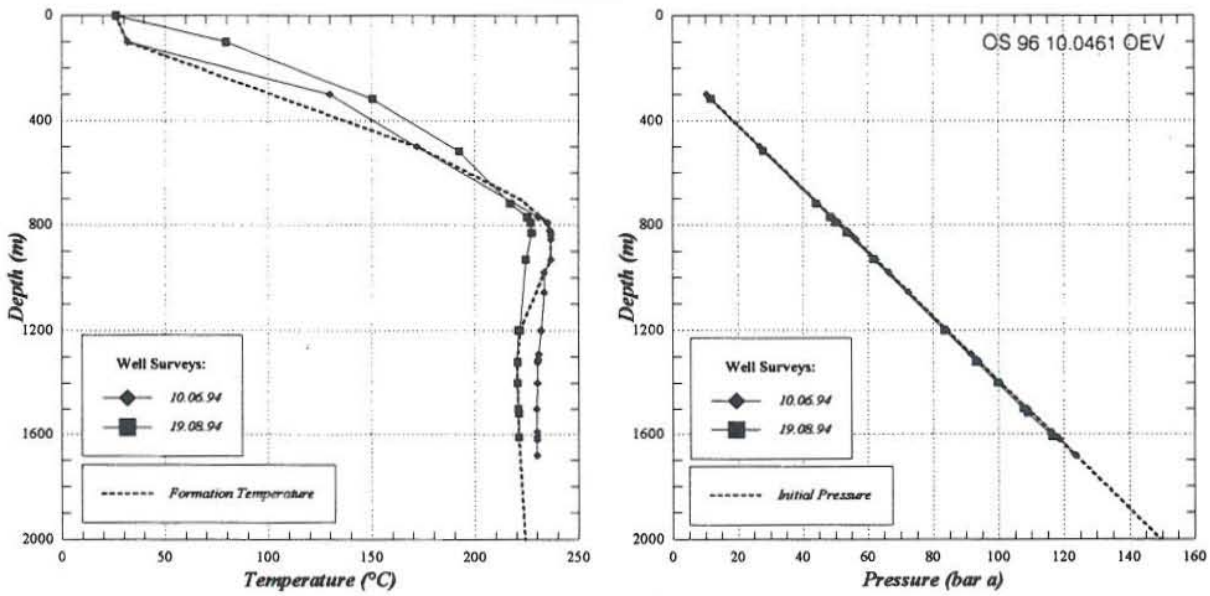

FIGURE 18: Formation temperature and initial pressure for well PGM-20

In **WELL PGM-21,** the estimated formation temperature and initial pressure are based on the 01.09.93 surveys, which are assumed to be the most confident static profiles (Figure 19). However, the deepest part of the well can be affected by down-flow conditions. The formation temperature in the zone from 500-1000 m depth is slightly modified in the temperature survey.

WELL PGM-22 is in down-flow conditions during shut-in. It receives all the reinjection water from one of the separator units, but is expected to be used as a production well in the near future. The estimated formation temperature is based on the 12.02.93 survey. The liner hanger is located at 836 m depth, so the temperature is corrected in the 800-1000 m depth range for a convection effect in that zone but also in the 1000-1300 m depth zone. A slight temperature reversal in the survey is considered to be true. The 24.10.94 survey is taken as the initial pressure (Figure 20).

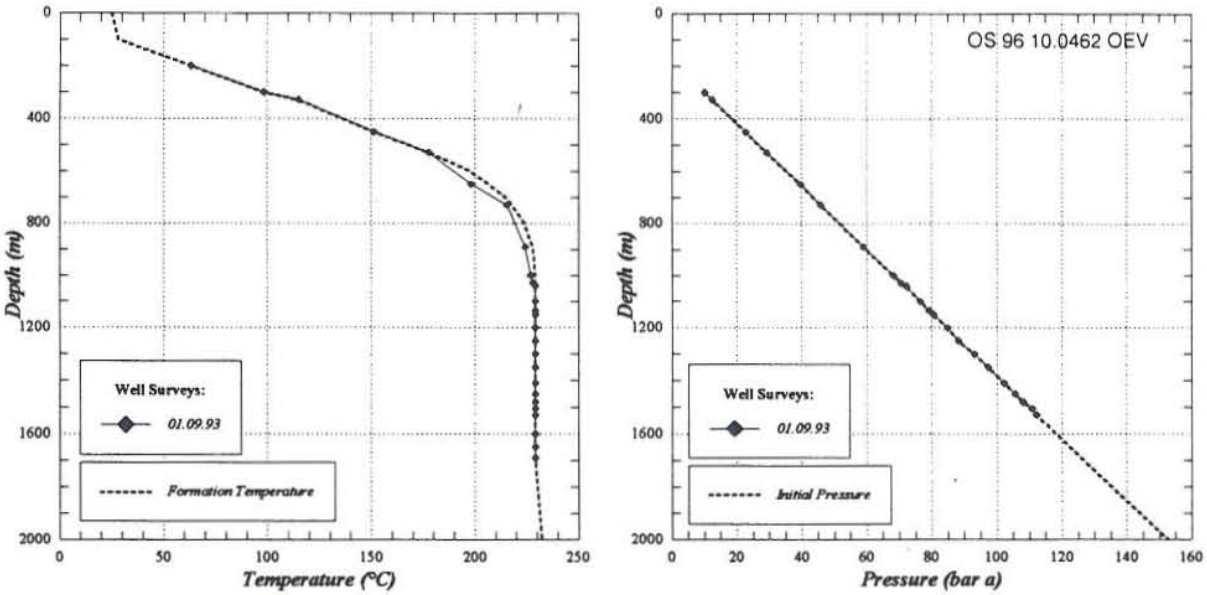

FIGURE 19: Formation temperature and initial pressure for well PGM-21

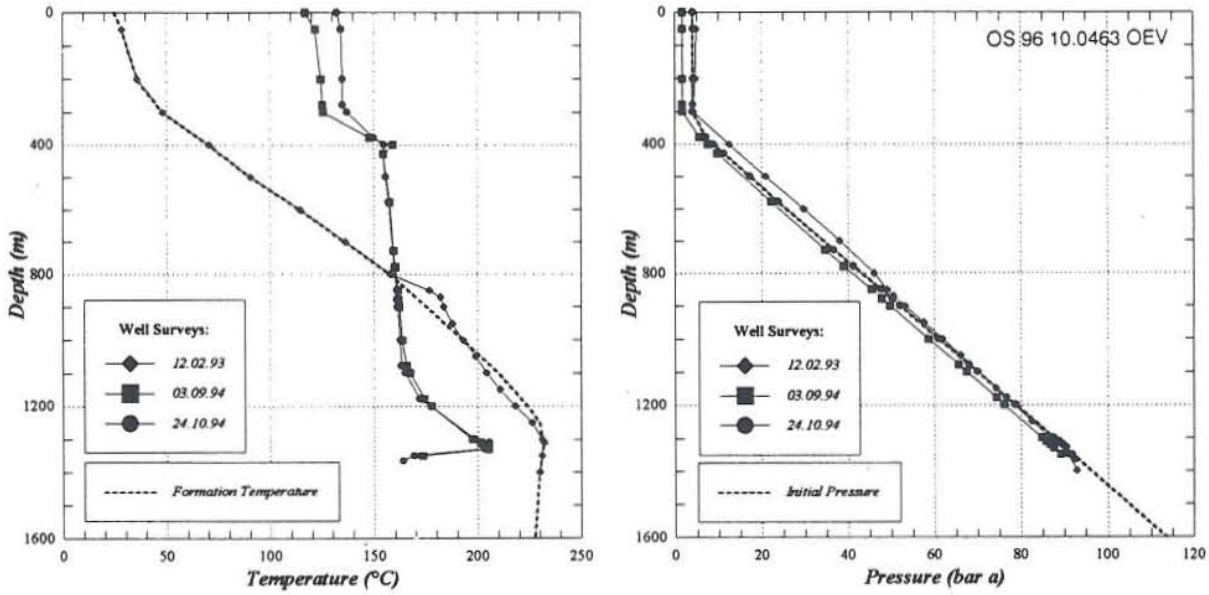

FIGURE 20: Formation temperature and initial pressure for well PGM-22

WELL PGM-24, similar to well PGM-22, receives all its water from one of the separator units, but is expected to be used as a production well in the near future. The estimated formation temperature is based on the 19.12.93 measurement, correcting the temperature in the 500-900 m depth range for some convecting effects in the well. The temperature in the deepest part of the well may be affected by down-flow conditions and a temperature reversal is considered to be true. The estimated initial pressure is based on the 19.12.93 survey (Figure 21).

WELL PGM-25 presents a low-temperature condition (under 200°C) and is treated as a boundary well. The formation temperature was estimated by using the program BERGHITI because in this well the static surveys allow a temperature recovery analysis. The initial pressure is based on the 12.11.94 survey (Figure 22).

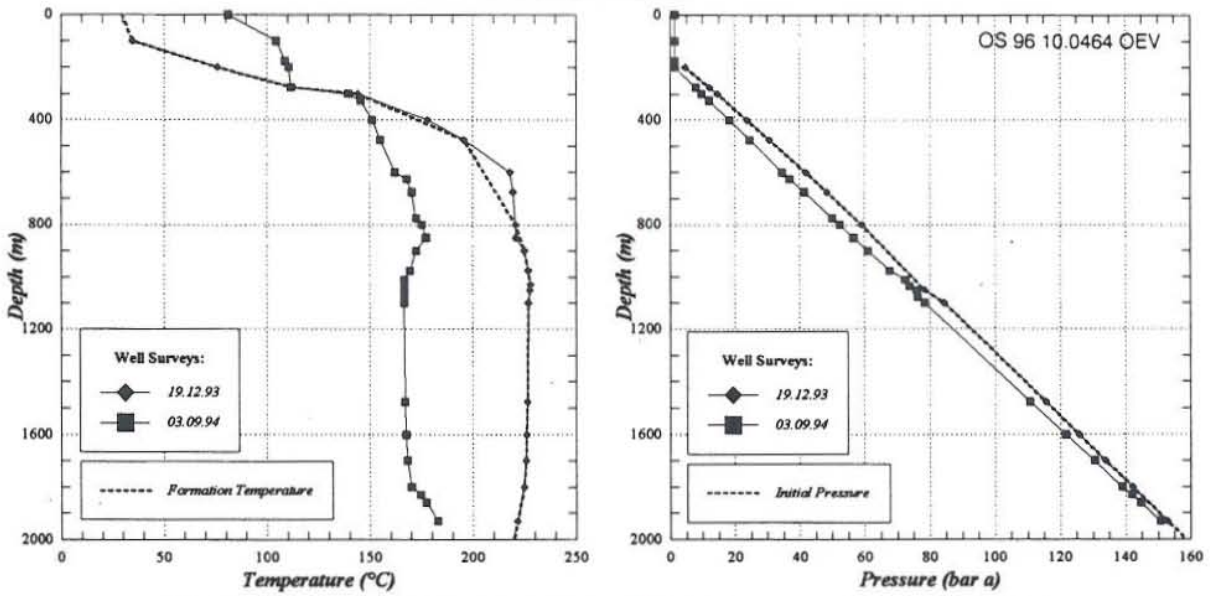

FIGURE 21: Formation temperature and initial pressure for well PGM-24

WELL PGM-26 was drilled as a reinjection well. The 07.08.93 survey is considered as the formation temperature, and the shallow aquifer is estimated to be about 50 m thick. The 22.11.95 survey is set as the initial pressure (Figure 23).

WELL PGM-27 was drilled to complete the requirements for the reinjection, but is actually not in use because the rest of the reinjection wells accept all the reinjection water. The estimated formation temperature and the initial pressure are based on the 06.12.95 surveys. However, the temperature in the 900-1400 m depth range is considered to be hidden by down-flow in the well. For this reason a temperature reversal is set in this range (Figure 24).

WELL PGM-28 was drilled as a reinjection well for the second unit, but proved to be a very good production well. The estimated formation temperature and the initial pressure follow the 14.11.94 surveys. This well is not affected by down-flow conditions, and the measured temperature in the deepest part of the well is considered to be a true formation temperature (Figure 25).

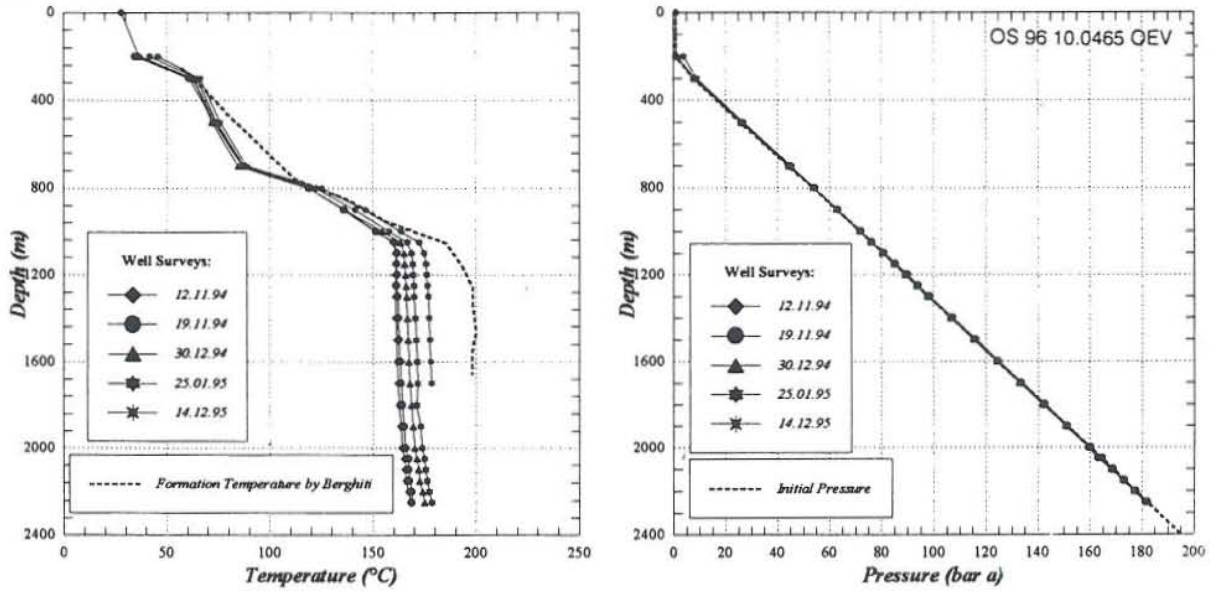

FIGURE 22: Formation temperature and initial pressure for well PGM-25

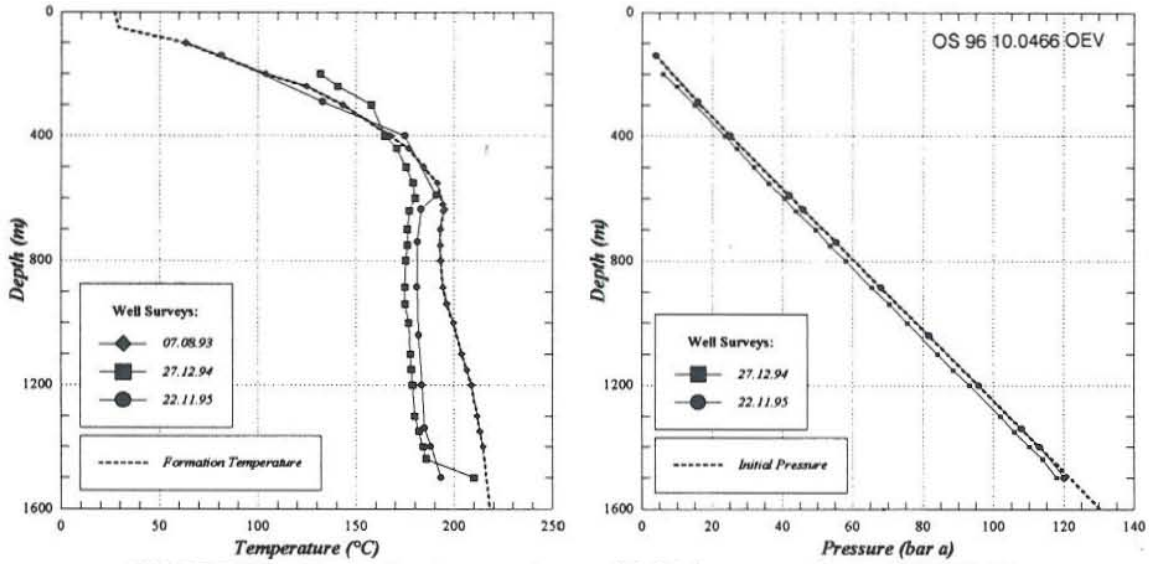

FIGURE 23: Formation temperature and initial pressure for well PGM-26

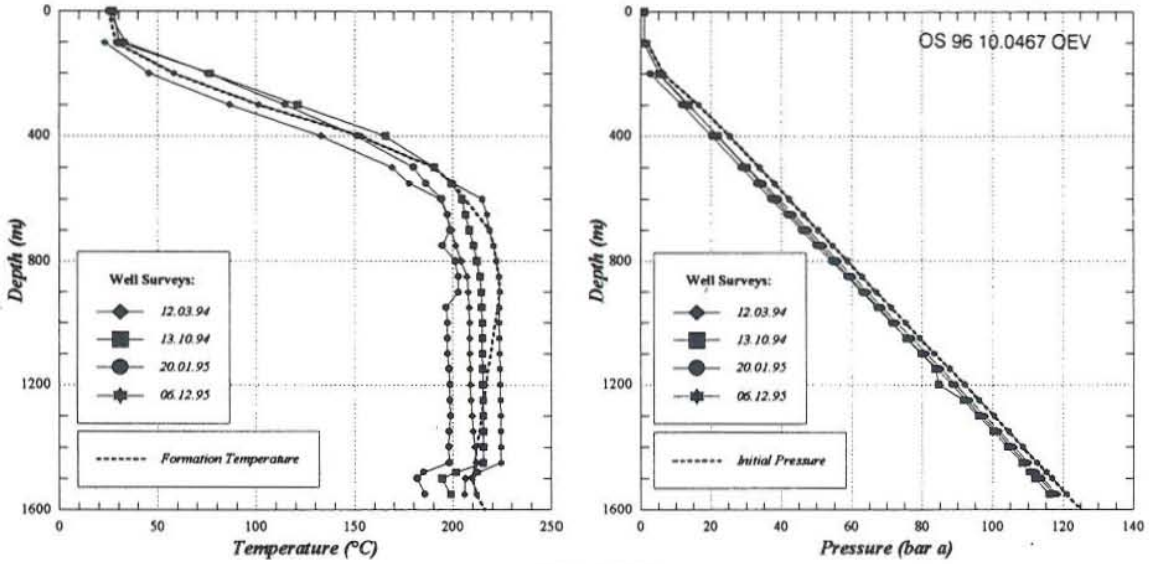

FIGURE 24: Formation temperature and initial pressure for well PGM-27

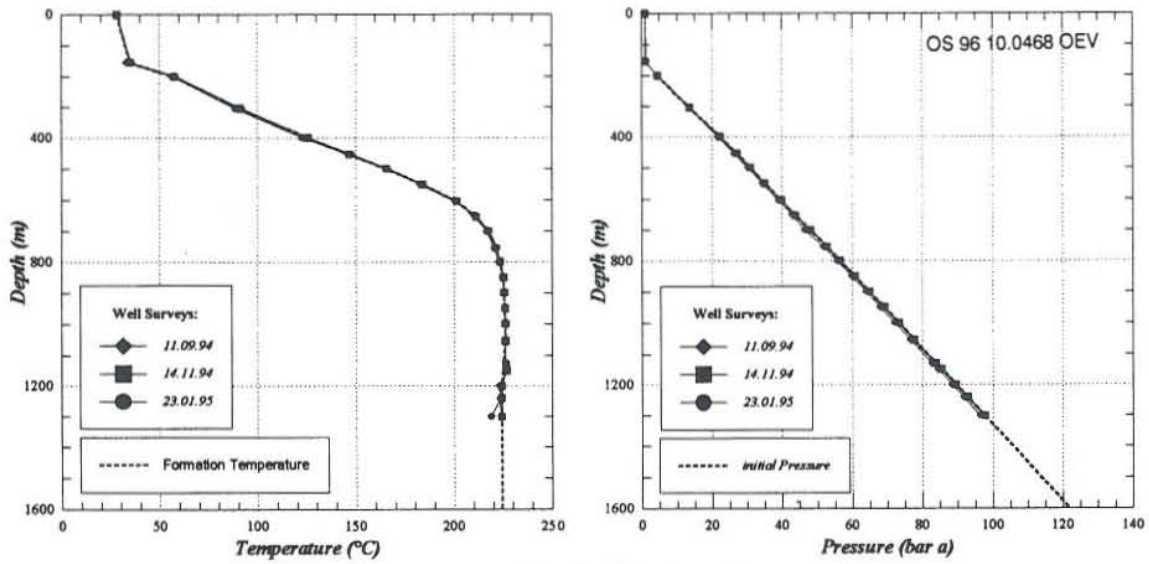

FIGURE 25: Formation temperature and initial pressure for well PGM-28

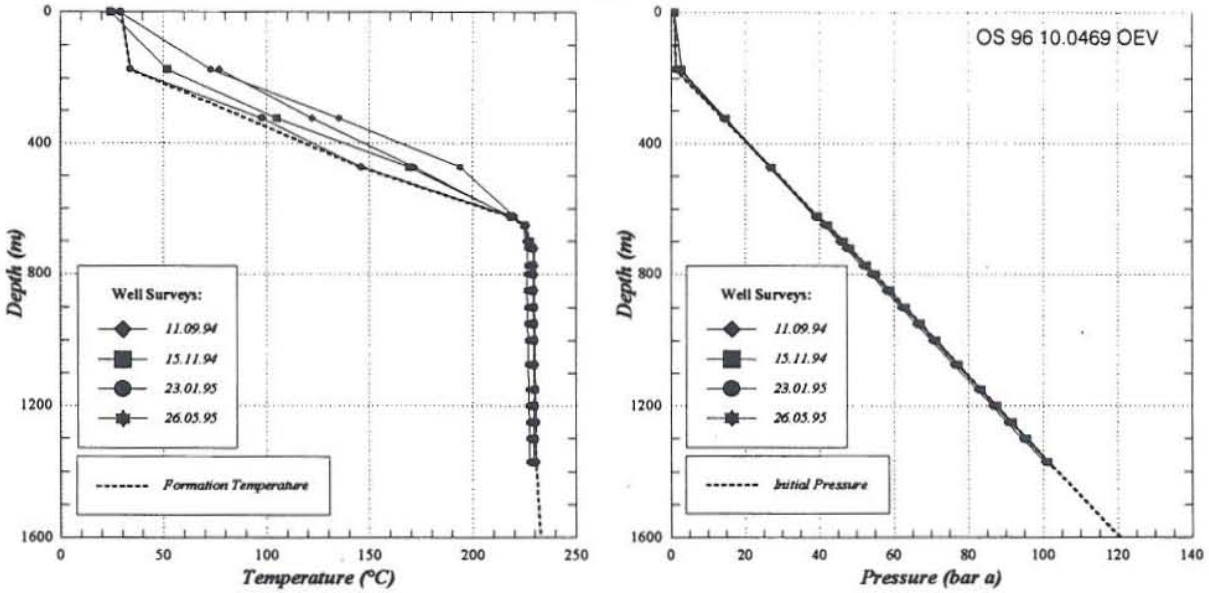

FIGURE 26: Formation temperature and initial pressure for well PGM-29

WELL PGM-29 is, similar to well PGM-28, a very good production well, but will be used as a reinjection well for the second unit. The estimated formation temperature is based on the 23.01.95 survey. A small increase of 2°C in the temperature at the bottom hole is taken to be true. The 23.01.95 survey is the basis for the estimated initial pressure (Figure 26).

WELL PGM-31 presents down-flow conditions during shut-in. The estimated formation temperature is mainly based on the 17.09.94 survey, and the 06.02.93 survey for the temperature reversal zone. In the 0-800 m depth range some corrections are made in order to correct for convections effects. The 06.02.93 survey is used as an initial pressure estimate (Figure 27).

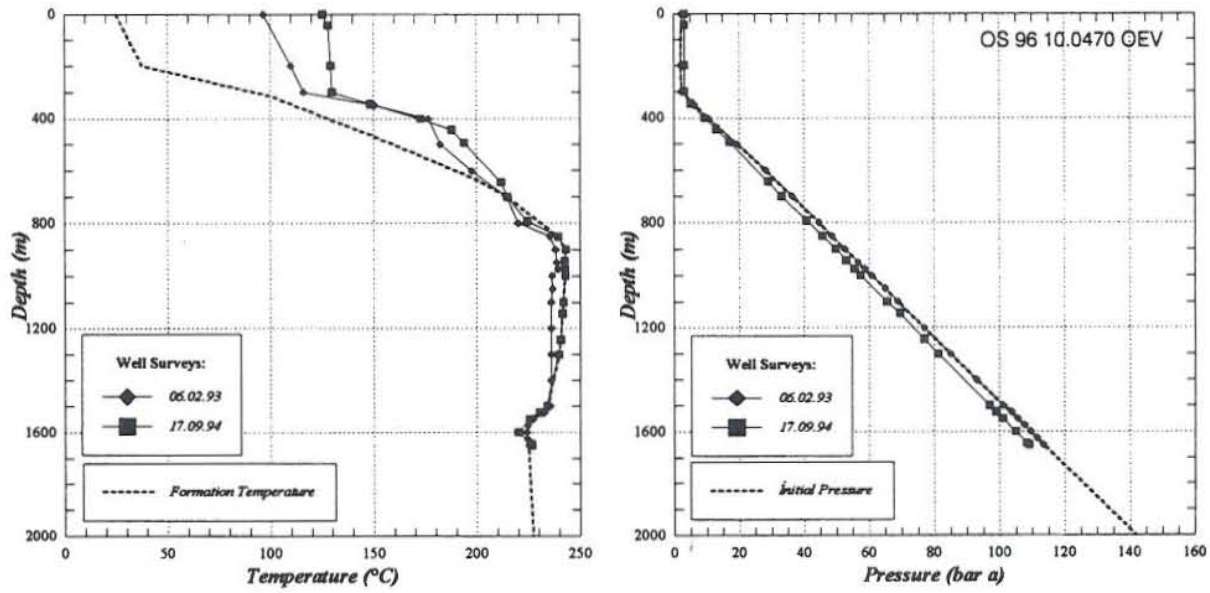

FIGURE 27: Formation temperature and initial pressure for well PGM-31

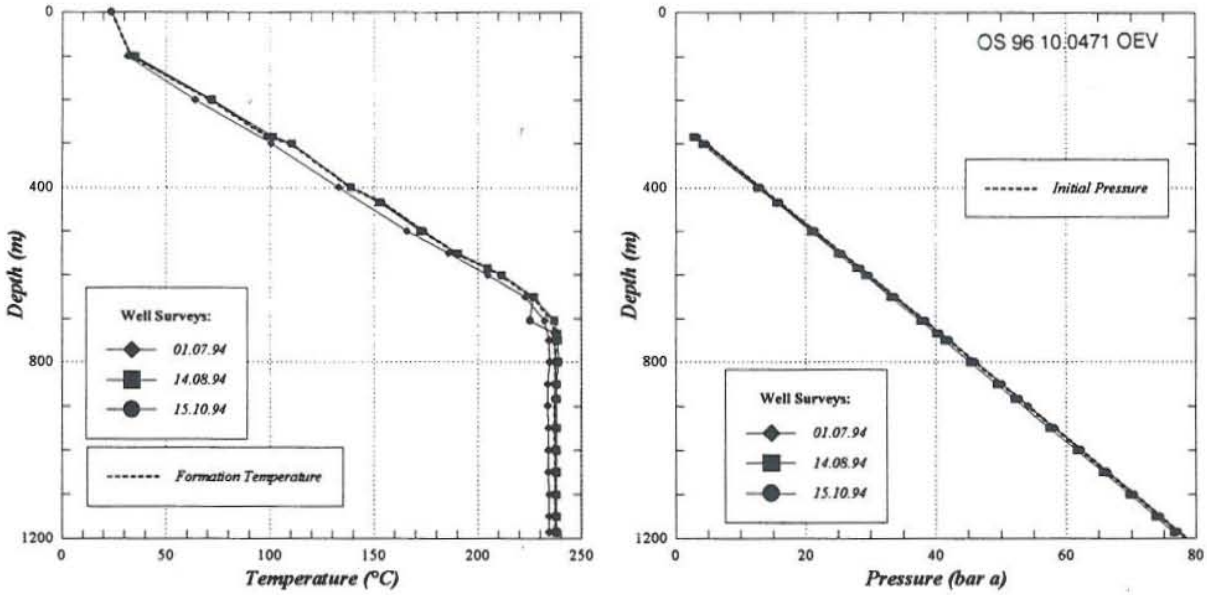

FIGURE 28: Formation temperature and initial pressure for well PGM-46

WELL PGM-46 was drilled as a production well for the second unit, but is presently supplying steam to the first unit. The 15.10.94 surveys are taken as the estimated formation temperature and initial pressure profile. The downhole temperature is considered true in the deepest zone of the well, because no down-flow conditions have been detected (Figure 28).

4. A CONCEPTUAL RESERVOIR MODEL

The formation temperature and the initial reservoir pressure before exploitation shown in the past paragraphs serve as a foundation for the Miravalles conceptual reservoir model. In Figure 29 are shown the formation temperatures and reservoir pressure distribution at -100 m a.s.l. Figures 30 and 31 show temperature cross-section through the field from south to north (A-A´) and from west to east (B-B´). More temperature and pressure contour maps and cross sections are presented in the Appendix.

From the contour maps it is deduced that the geothermal fluid flow primarily follows a NE-SW direction with a change to the N-S direction in the central part of the field. Fluid flow appears to come from the vicinity of wells PGM-10 and PGM-11, where the highest temperatures and pressures in the field are observed. The temperature and pressure descend gradually to the south, from a maximum near well PGM-11 (around 251°C) to around 220-230°C in wells PGM-26 and PGM-16. The reservoir is clearly bounded to the west due to the low temperatures and pressures observed there (wells PGM-04, 15, and 22). To the east the contour plots are open, due to lack of data in that part (Figure 29).

Relating the main features of the Miravalles field and the analysis of the formation temperature, initial pressure and their distribution in the field, a conceptual model is presented as follows:

The Miravalles reservoir has a main inflow of 250-260°C fluid coming from the northeastern part of the well field, near well PGM-11. The inflow zone of the field is related to the Miravalles volcano, which may serve as the heat source for the hot inflow fluid. The fluid flows laterally from north to south, as can be seen in the temperature and pressure distribution of the field. The lateral flow zone causes for example, the temperature reversal observed in many wells. This zone can be associated with some

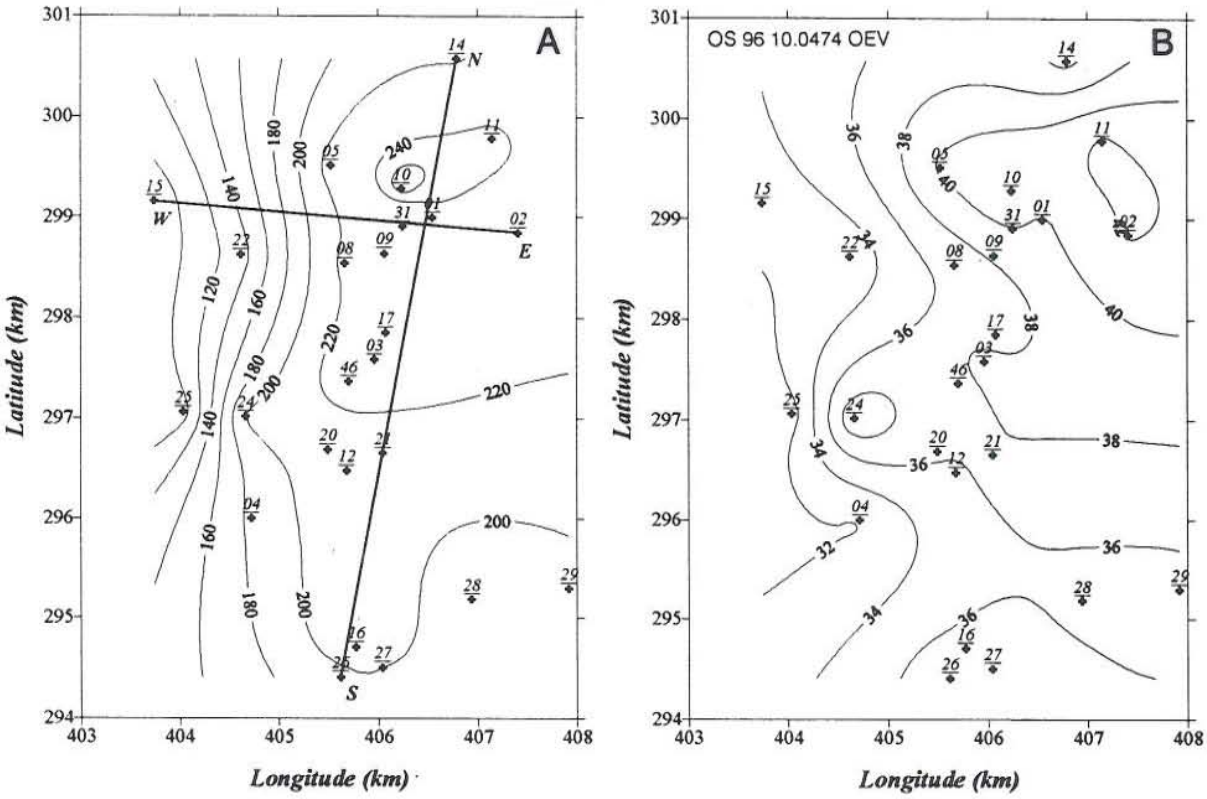

FIGURE 29: Temperature (°C) and pressure (bar-a) contour maps at -100 m a.s.l.

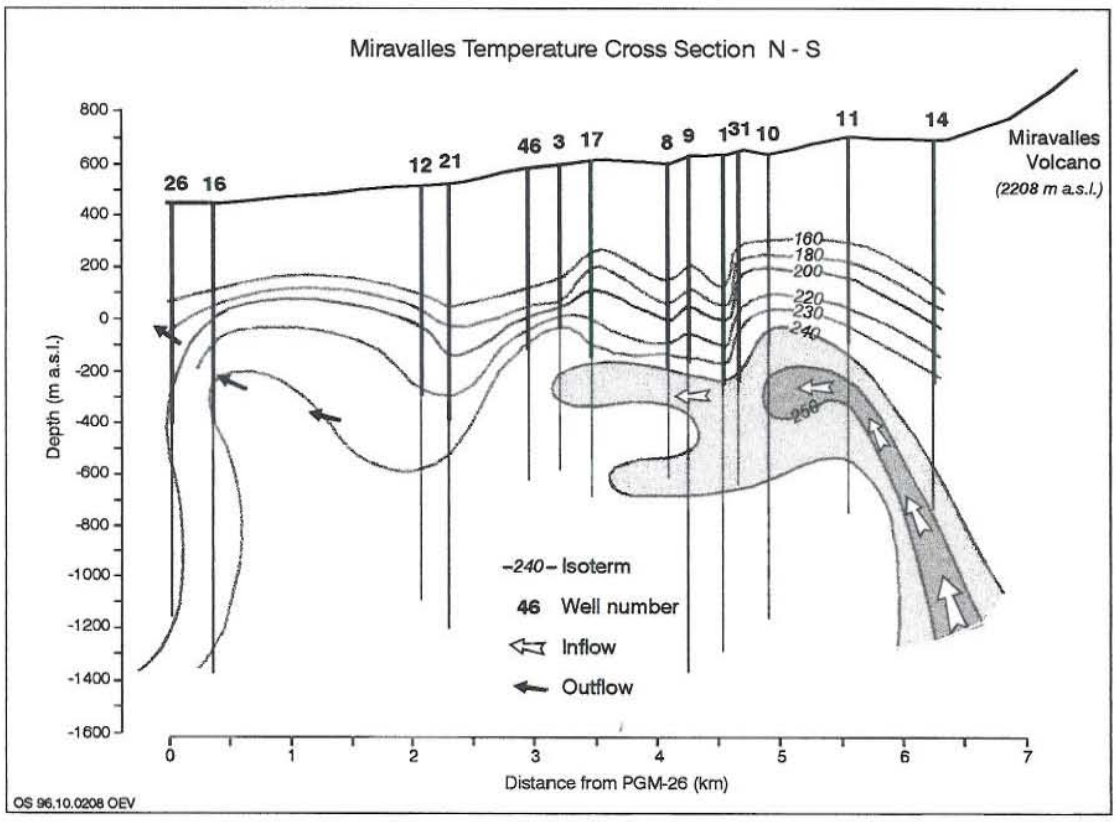

FIGURE 30: A S-N temperature cross-section through the Miravalles field

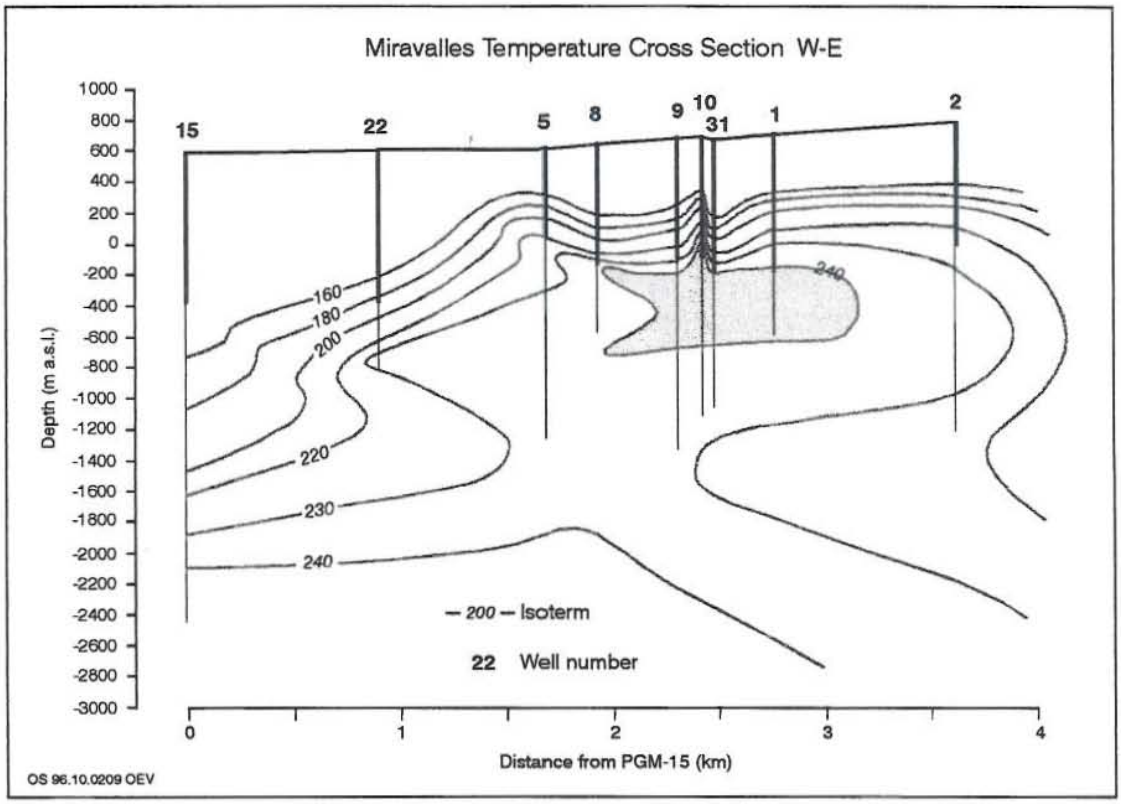

FIGURE 31: A W-E temperature cross-section through the Miravalles field

sedimentary units (Chapter 2.2.1). The main outflow is at the south of the field, near wells PGM-16, PGM-26 and PGM-27.

A closed boundary is clearly observed in the western part of the well field. The temperature decreases rapidly in this part, as does the pressure. The reservoir is open to the north (inflow) and south (outflow). The reservoir seems to continue to the east, but the extension cannot be estimated clearly because there are no wells in that region.

5. RESERVOIR MODELLING TECHNIQUES

An important part of an assessment of a geothermal field is the development of a mathematical model of the field. The main purpose of developing such a model is to help in the decisions taken during the operation of the reservoir. In accordance with the level of modelling realized, the performance of a geothermal reservoir can be predicted under different exploitation conditions and production potential. The accuracy of the mathematical model is related to the modelling techniques used, the amount of field data collected over the years and the number of different variables used. The modelling techniques can be grouped into two main categories: simple lumped modelling and distributed parameter modelling. The simple modelling techniques are reduced cost and time alternatives. They simplify the geometry and the properties of a reservoir and simulate the response of one of a few selected variables (pressure, temperature or chemistry). The distributed parameter modelling techniques are complex tools which simulate many measurable variables. They require accurate geometries and extensive field data (Axelsson, 1996).

In the following sections two different models are used to simulate the Miravalles field data. One of the models is the lumped parameter model LUMPFIT (Axelsson and Arason, 1992). The other is the TOUGH simulation code (Pruess, 1987).

5.1 Lumped modelling

Lumped parameter modelling is a simple method where the reservoir is modelled in different parts, each of them having some determined hydrological properties. Those properties are lumped together, simplifying the reservoir characteristics into a few dependent variables (Axelsson and Arason, 1992). The method consists of developing a network which simulates the reservoir behaviour. This network consists of some capacitors or tanks that are connected by resistors, each capacitor having a mass capacitance, κ. The capacitor responses with increased pressure when a load of liquid mass m is given in the system in the form $p = m/\kappa$. The mass conductance of each resistor σ, controls the liquid flow q, due to an impressed pressure differential Δp by $q = \sigma \Delta p$. This network can be open or closed to a constant pressure boundary (Axelsson, 1989). In general, the capacitors simulate the storage of different parts of the reservoir and the resistors the corresponding permeability.

The pressure response p, in an open N-tanks lumped model, to a constant production Q, starting time $t = 0$ is given by

$$p(t) = -\sum_{j=1}^{N} Q \frac{A_j}{L_j}(1 - e^{L_j t}) \qquad (1)$$

For a closed N-tanks lumped model with a production rate of Q at time $t = 0$, the pressure response p is given by

$$p(t) = -\sum_{j=1}^{N-1} Q \frac{A_j}{L_j}(1 - e^{L_j t}) + Q B t \qquad (2)$$

The coefficients A_j, L_j and B are dependant on the value of the related tank storage coefficient κ_j and conductance coefficient of the resistor σ_j of the model (Axelsson and Arason, 1992). In a geothermal system the capacitance of the capacitor is related to the storativity s of the reservoir, the volume V_j and the reservoir fluid density ρ by $\kappa_j = V_j s \rho$ (Quijano, 1994). The storativity index is dependent on the reservoir type. An automatic, least squares inversion program, LUMPFIT, is available for solving the unknowns A_j, L_j and B in Equations 1 and 2, given the pressure and production history of the reservoir (Arason and Björnsson, 1994).

5.2 Three-dimensional numerical modelling

The numerical modelling method consists of simulating the reservoir as a number of subvolumes, each of them having determined hydrological, thermodynamic and chemical properties. Those properties are set according to the measured data observed during the reservoir assessment, and change throughout the reservoir exploitation. In such a condition, simplifying the reservoir characteristics does not make sense, as the purpose of the numerical modelling is to have a reservoir model as close to reality as possible. The modelling is made using not only the data available, but also analytical and empirical equations that represent the real behaviour of the different components of the mass, rock, etc. The simulation is run in high velocity computers because of the high number of variables involved. The program TOUGH is one of those numerical models.

The basis of TOUGH is the same as normally applied in geothermal reservoir simulators. The mass- and energy-balance equations for an arbitrary flow domain Vn, are written as shown in the next equation (Pruess, 1987):

$$\frac{d}{dt}\int_{V_n} M^{(\kappa)} dv = \int_{\Gamma_n} F^{(\kappa)} d\Gamma \times n\, d\Gamma + \int_{V_n} q^{(\kappa)} dv \tag{3}$$

where the coefficient κ is 1 for water flow, 2 for air flow and 3 for heat flow.

The mass accumulation terms for κ being 1 or 2 is related to the porosity ϕ, the saturation S_β, density ρ_β and mass fraction $X_\beta^{(\kappa)}$ of component κ present in each phase β (liquid or gas) in the form

$$M^{(\kappa)} = \Phi \sum_{\beta=l,\, g} S_\beta \rho_\beta X_\beta^{(\kappa)} \tag{4}$$

The rock and fluid contribute to the heat accumulation term in the form

$$M^{(3)} = (1-\Phi)\rho_R C_R T + \Phi \sum S_\beta \rho_\beta u_\beta \tag{5}$$

where the different terms describe the following: ρ_R is rock grain density, C_R is specific heat of the rock grains, T is temperature and u_β is specific internal energy of phase β.

The mass flux terms contain a sum over phases

$$F^{(\kappa)} = \sum_{\beta=l,\, g} F_\beta^{(\kappa)} \tag{6}$$

and the flux in each phase is related to the absolute permeability k, relative permeability, viscosity and pressure of phase β, $k_{r\beta}$, μ_β, $P_\beta = P + P_{cap,\beta}$ and the gravitational acceleration g as

$$F^{(\kappa)} = -k\frac{k_{r\beta}}{\mu_\beta}\rho_\beta X_\beta^{(\kappa)}(\nabla P_\beta - \rho_\beta g) - \delta_{\beta g} D_{va}\rho_\beta \nabla X_\beta^{(\kappa)} \tag{7}$$

Heat flux is by conduction and convection in the rock-fluid mixture, and is related by the heat conductivity of the rock-fluid mixture K and the specific enthalpy of the component κ in phase β as follows:

$$F^{(3)} = -K\nabla T + \sum_{\substack{\beta=l,\, g \\ \kappa=1,\, 2}} h_\beta^{(\kappa)} F_\beta^{(\kappa)} \tag{8}$$

Equation 1 discretized in space using the integral finite difference, using an appropriate volume, averages

$$\int_{V_n} M\, dv = V_n M_n \tag{9}$$

In the above equation, M describes a volume-normalized extensive quantity and M_n is the average value of M over V_n. It is convenient to approximate the surface integral as a sum of averages over surface segments A_{nm} as follows:

$$\int_{\Gamma_n} F \times n \, d\Gamma = \sum_m A_{nm} F_{nm} \tag{10}$$

Time is discretized for obtaining a numerical stability necessary for a correct calculation of multi-phase flow. Finally, Equation 1 is reduced to the following equation:

$$R^{(\kappa)k+1} \equiv M_n^{(\kappa)k+1} - M_n^{(\kappa)k} - \frac{\Delta t}{V_n} \left(\sum_m A_{nm} F_{nm}^{(\kappa)k+1} + V_n q_n^{(\kappa)k+1} \right) = 0 \tag{11}$$

where k represents a time step $\Delta t = t^{k+1} - t^k$. For a flow system which is discretized into N grid blocks, Equation 11 represents a set of $3N$ algebraic equations. TOUGH develops a simultaneous solution of these equations (mass- and energy-balance equations).

6. MODELLING OF THE MIRAVALLES GEOTHERMAL FIELD

6.1 Lumped reservoir model

Figure 2 shows the total production and pressure history of the Miravalles field. This data serves directly as input for the lumped modelling studies. However, one important change is needed. As all the separated fluid is reinjected, one must assume that only the steam fraction corresponds to the net production. Change in drawdown rate in well PGM-09, after the beginning of production of PGM-31, required a division of the production history into early data and late data. A simulation of the whole data history was also carried out. The production data shown in Figure 2 was simulated as follows:

1. Production and pressure drawdown data were simplified as is shown in Figure 32. Only net production (steam mass flow) was used in the simulation. It is assumed that all the reinjected water returns to the reservoir. Production prior to the continuous mass extraction was neglected.
2. The early data were taken from the beginning of the continuous production to the start of production from well PGM-31. The time period of inversion used in the lumped model was thus 360 days. The initial pressure at 241 m a.s.l. was estimated 10.1 bar-a.
3. The late data period starts on day 210 and continues to day 456. For fitting the model, a higher initial pressure was guessed, at 241 m a.s.l. it was supposed to be 10.5 bar-a.
4. The whole data set on Figure 32 was finally used to constrain a lumped model. The initial pressure was

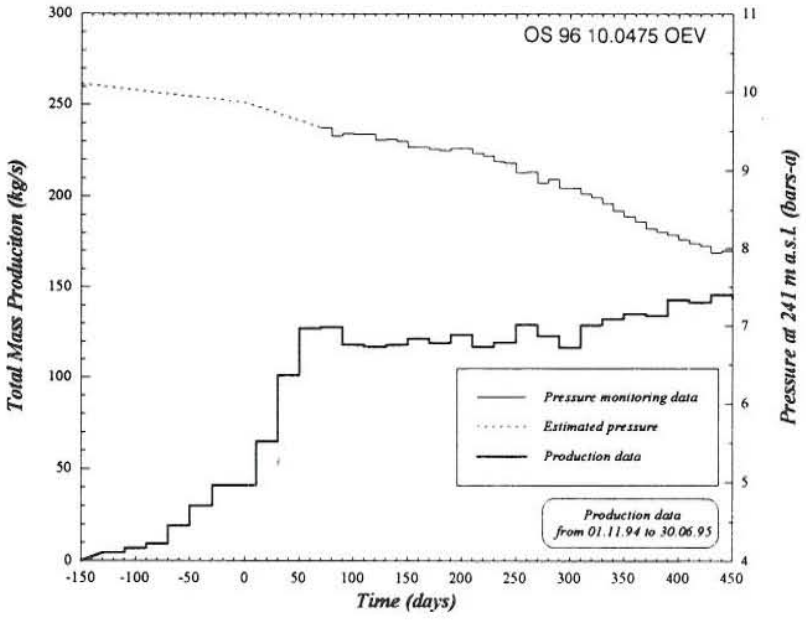

FIGURE 32: Net mass extraction of Miravalles and pressure drawdown at 241 m a.s.l.

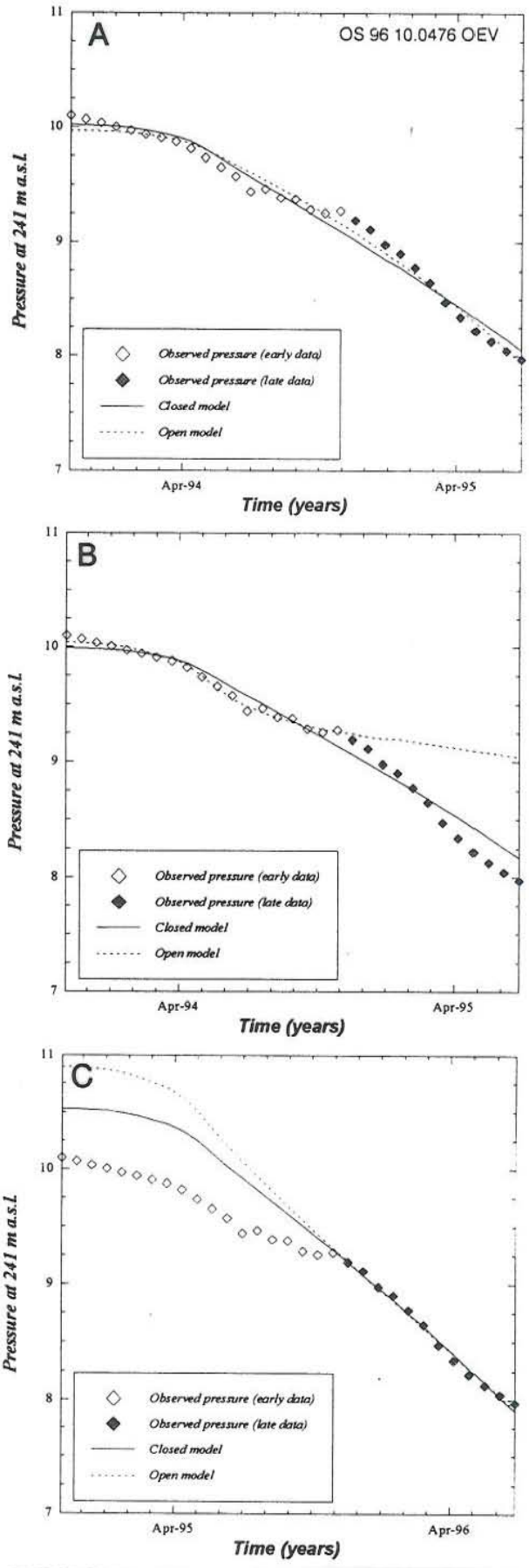

FIGURE 33: Measured and calculated pressures for the different time intervals, a) whole data; b) early data; c) late data

considered to be 10.1 bar-a.

The simulations were carried out using one-tank closed and one-tank open models, for each of the three different cases. The results of the modelling are shown in Table 4 and graphically in Figure 33. The matches between observed and calculated pressures are quite good, giving determination coefficients over 98% for all cases except in the closed-tank model for early data. The calculated and measured data generally deviate around 0.03-0.09 bar. The open-tank model fits the early data drawdown better. Both open- and closed-tank models fit the late data quite well. For the whole data set, both open- and closed tank models fit the data, but the open-tank model shows an unrealistic σ negative value. This value does not have any physical meaning and makes this operation model useless for predictions.

Figure 34 shows the matches for the three models used and also the predicted pressure conditions at 241 m a.s.l. for a 2000 day period (five years). These predictions were made for 100, 150, 200 and 250 kg/s of net production. The 150 kg/s value is near to the present net mass extraction rate, and the 250 kg/s value is close to the future net mass extraction, when the second power plant starts operation. The future pressure response is quite similar for almost all cases, except the open tank models. They converge to stable pressures after either a few months or years of production. For the rest of the cases a fast drawdown is predicted, between 2 to 52 bars (this last value corresponds to the whole data open-tank model) in 4 years for a net production in the range 100-250 kg/s. In some cases the calculated pressures reach negative values, but do not make any real sense. That situation occurs when the water level in the monitoring well falls below the position of the monitoring probe.

The monitoring in well PGM-09 is still continuous. Pressure drawdown data are available until January 1996. Comparing

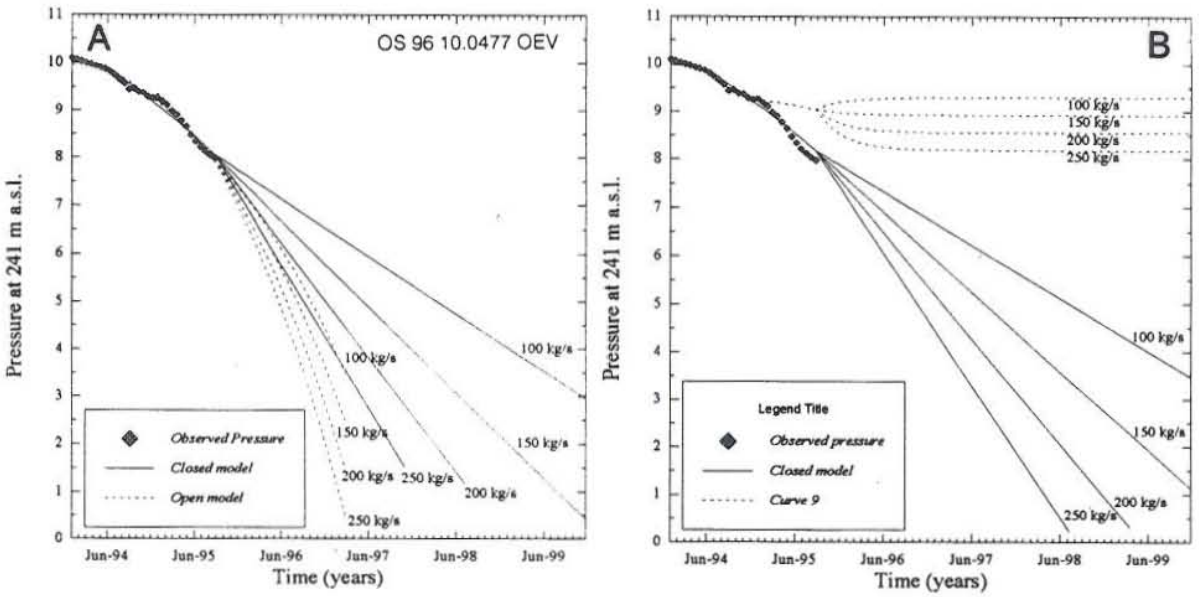

the last monitoring value with the different production scenarios in Figure 34 suggests that the Miravalles field may still behave as a closed-tank system.

The lumped modelling presented here simulates the past and provides predictions for the future pressure behaviour of the field. It should be noted that the model does not consider temperature changes or expansion of boiling in the reservoir due to massive exploitation. The rapid pressure drawdown at the present time follows a liquid-dominated storativity, but may change progressively to a steam storativity, because of increased boiling in the reservoir. Hence, the model will only be useful until that occurs. Another source of concern is the destiny of the reinjected water. If only a fraction of it enters the productive wellfield the net production rates are much larger than assumed here.

FIGURE 34: Prediction of the future reservoir pressure for the different models, a) whole data; b) early data; c) late data

TABLE 4: Properties of lumped parameters models for the Miravalles production history

Period	Early data		Late data		Whole data	
Model type	**Closed**	**Open**	**Closed**	**Open**	**Closed**	**Open**
Po	9.99	10.04	10.53	10.50	10.02	9.97
B	0.303E-4	---	0.439E-4	---	0.328E-4	---
A(1)	---	0.688E-4	---	0.652E-4	---	0.239E-4
L(1)	---	0.928E-2	---	0.125E-2	---	-0.147E-2
κ	28518.7	12550.6	19698.7	13243.0	26342.5	36214.8
σ	---	0.135E-2	---	0.191E-3	---	-0.603E-3
Coeff. of det. (%)	95.08	99.14	99.22	99.29	98.10	98.67
Standard dev. (bar)	0.067	0.029	0.040	0.040	0.091	0.077

6.2 Three-dimension natural state model

The grid designed for three-dimensional numerical modelling is shown in Figure 35. It is formed by three reservoir layers (GRA, GRB and GRC) of 58 blocks per layer. A special layer simulates the basement of the reservoir (BAS). This layer has only 13 blocks, connected vertically to layer GRC. Similarly, on top of layer GRA is another layer, CAP. These layers account only for heat conduction. Each of the layers GRA, GRB and GRC are 400 m thick. The wellfield blocks are 1 km^2 in area, giving a total area extend of 42 km^2. The rest of the blocks are substantially larger than the wellfield blocks and serve as boundary blocks.

The rock properties, in the TOUGH model are divided into 6 domains: boundary blocks, high- medium- and low-permeability blocks, inflow blocks and outflow blocks. Their physical properties are given in Table 5. The boundary blocks simulate the conditions in the boundaries of the field, especially in the well defined boundary to the west of the field, where the temperature and pressure descend drastically. The high- and low-permeability blocks simulate zones where the permeability is high or low, respectively. Permeability selection is related to the flow paths identified in the definition of the Miravalles conceptual model (Chapter 4), where it is seen that the flow runs from north to south, following a channel in the central part of the field, but has poor flow movement in the western part. The high-permeability blocks in this model allow the fluid to flow from the inflow zone in the north to the outflow zone in the south. The inflow blocks have high vertical permeability which simulates the Miravalles volcano deep recharge. According to the conceptual model these blocks are located in the vicinity of wells PGM-10, PGM-11 and PGM-14. The outflow blocks simulate the discharge of colder fluids of Miravalles. They are located in the vicinity of well PGM-26, according to the conceptual model. In this case the outflow is absorbed by a vertical row of blocks of very large volume.

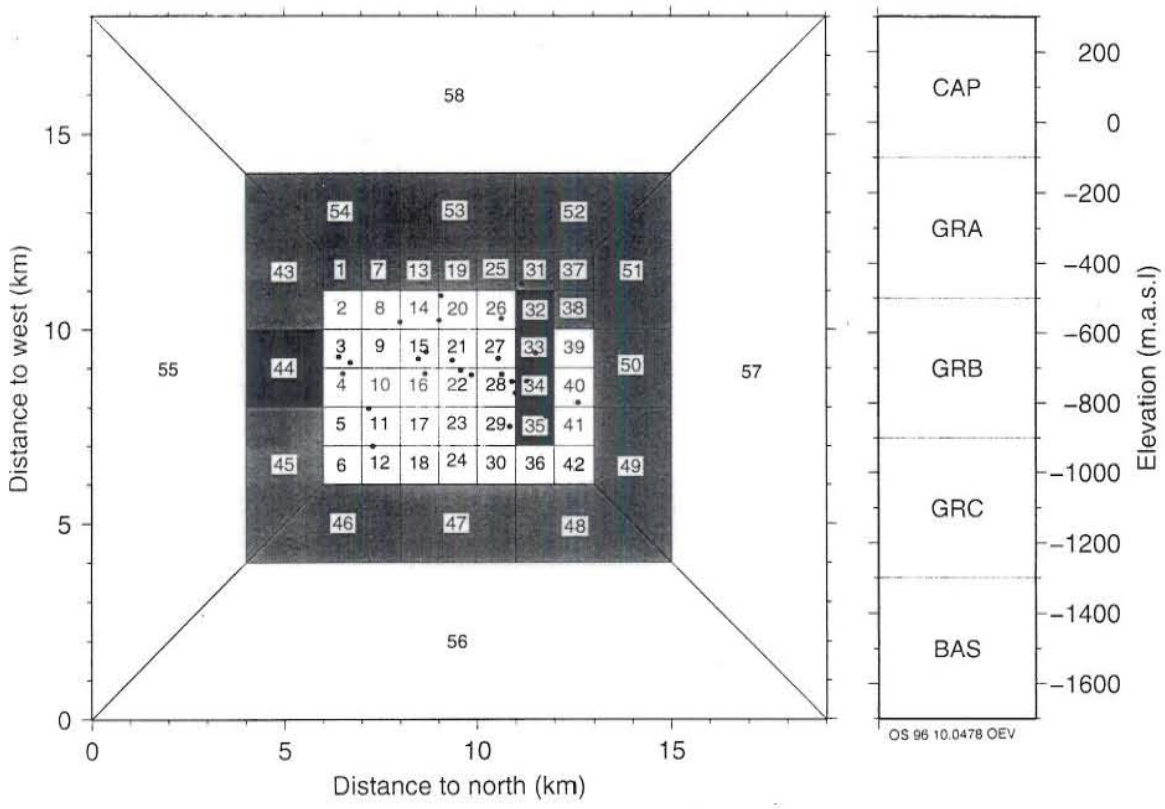

FIGURE 35: A TOUGH grid layout for the Miravalles field, light grey denotes *bound* blocks, middle grey denotes *welf2* blocks, and white blocks are *welf1*; block 44 simulates subsurface discharge to the south and blocks 32-35 simulate vertical recharge;wells are shown in black dots

The main parameters which define each rock type are the permeability in the different axes (directions), the thermal conductivity of the formation and the specific heat of the rock. In the natural state simulation the porosity does not play an important role. The *welf1* represents the high-permeability rocks, located in the central part of the well field, where the conceptual model indicates the flow path. The *welf2* are the low-permeability rocks. These are the western part of the field. The *welf3* are mainly the blocks situated in the inner layers of the model (GRB and GRC), which are rocks of medium permeability. This differentiation has the objective of promoting the fluid flow mainly in layer GRA, which is the top layer of the reservoir. The *verti* rocks are rocks with a high vertical permeability, which promotes the inflow of hot fluid from depth. At the same time the *outfl* are the rocks related with the outflow zone. The boundary rocks are rocks with negligible permeability and thermal conductivity, and high specific heat and volume. This forces the model to have stable pressure and temperature conditions in the boundaries of the reservoir.

TABLE 5: Rock properties for the TOUGH model

Rock name	Permeability in x-axis (m^2)	Permeability in y-axis (m^2)	Permeability in z-axis (m^2)	Thermal conductivity (W/m°C)	Specific heat (J/kg°C)
welf1	120E-15	3E-15	10E-15	1.3	1000
wellf2	30E-15	3E-15	10E-15	1.3	1000
welf3	60E-15	3E-15	10E-15	1.3	1000
verti	120E-15	3E-15	500E-15	1.3	1000
outfl	120E-15	100E-18	120E-15	1.3	1000
bound	1E-25	1E-25	1E-25	0.08	1E+30

The simulations assume a warm-up time of 200,000 years. The initial condition for every block is defined according to the field data collected and the conceptual model, especially in the caprock and the basement layers, and also in the inflow and outflow blocks. The iterative process of matching the field data includes the definition of the number of inflow and outflow blocks and the corresponding inflow rates, the different permeabilities of the rocks and thermal conductivities. All these conditions were set in order to match the initial temperature and pressure distribution of the field.

The main results, although not complete, indicate that it is necessary to have a total mass recharge of 190 kg/s of 260°C water for heating the system to reservoir temperature. For this inflow four blocks are used in the deepest layer GRC. The outflow blocks selected are blocks 44 in the GRA, GRB and GRC layers. The pressure and temperature behaviour indicate that the boundaries in this model are too close to the wellfield, resulting in high conductive heat losses. That situation highly affects the temperature distribution as is shown in Figure 36, specially at the southern and western parts of the field. Abnormally low thermal conductivity in the model boundaries gives a reasonable match. This means that the boundary blocks are "mathematically" moved further away. The heat loss q is given by $k\Delta T/\Delta x$ where k is the thermal conductivity, and $\Delta T/\Delta x$ is the temperature gradient over a distance Δx. Reducing the value of k has the same effect of increasing the distance Δx to the boundary block. Fluid production rates of 0.5 kg/s from blocks 3, 4, 9, 10, 15, 16, 21, 22, 27 and 28 in layer GRA were allowed in order to heat more rapidly the shallow layer GRA. Figure 37 shows the results for selected wells.

It is beyond the scope of this training study to obtain a perfect fit to the field data. The numerical model simulates important features in the conceptual model such as temperature reversal in some wells. The numerical modelling is a very complex process, which needs considerable time in iterating and setting the correct initial and boundary conditions. The boundary conditions clearly demonstrate how strongly they effect the whole model. Another point of interest is the internal state of the Miravalles caprock. It appears reasonable to split the caprock into a higher number of blocks for accurate simulation of its influence on the reservoir.

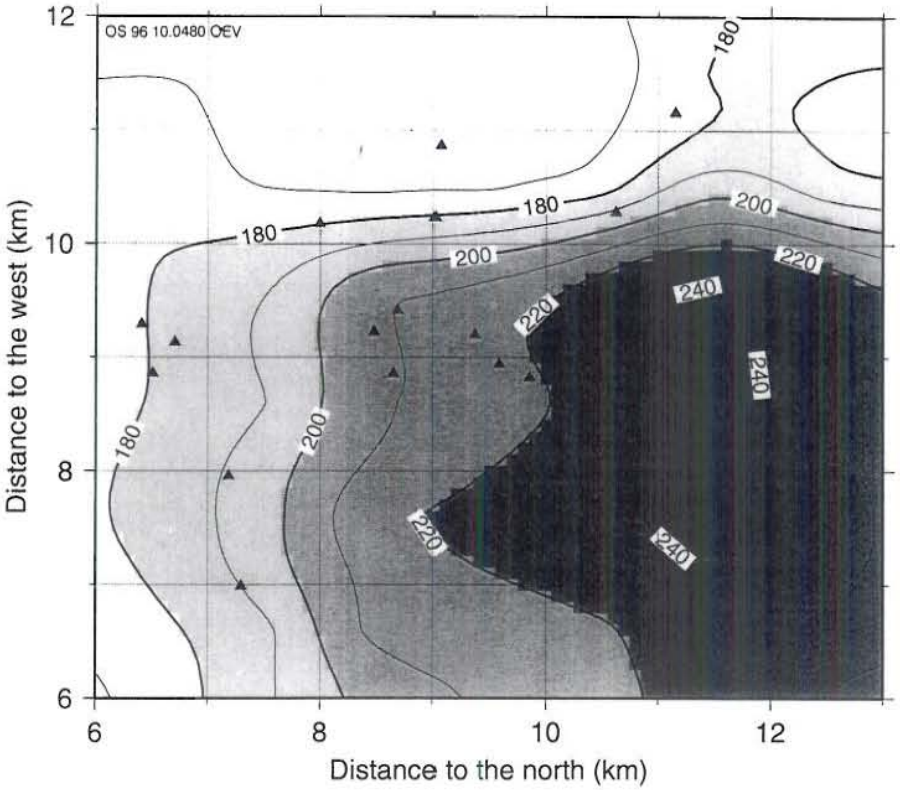

FIGURE 36: TOUGH simulation of temperature distribution in layer A

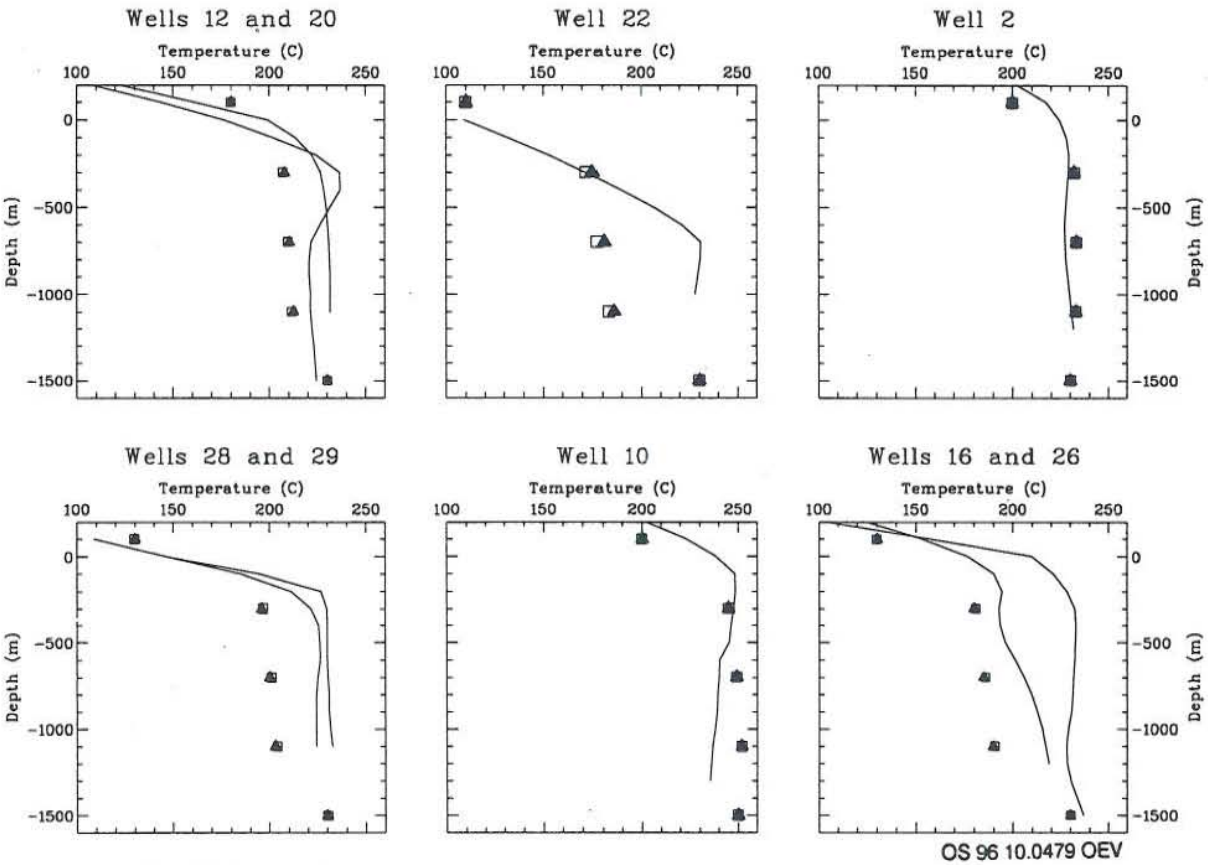

FIGURE 37: TOUGH simulation of formation temperatures for selected wells; the formation temperature for the different wells is shown as continuous lines and the TOUGH simulation as black dots

7. CONCLUSIONS AND RECOMMENDATIONS

The main conclusions of this study are as follows:

1. Total and net production and pressure history data for the Miravalles field have been collected and stored. Early pressure monitoring data is missing in the production history. A minimum of 10.1 bar-a initial pressure at -241 m a.s.l. in well PGM-09 was, however, estimated by using other data sources.

2. Downhole pressure and temperature data from twenty-five wells have been collected and analysed in terms of initial pressure and temperature profiles for each well.

3. The initial temperature and pressure distribution together with other information, define a conceptual model of the Miravalles reservoir. A 260°C upflow zone is proposed in the north, and a lateral flow zone at -100 to -300 m a.s.l. towards the south where subsurface discharge takes place. The wellfield is clearly bounded to the west by cold temperatures and low pressures. The character of the eastern boundary remains, on the other hand, unknown due to a lack of wells in the region.

4. Analysis of the production data using lumped models suggest that the Miravalles field will behave as a closed reservoir system for the next years, resulting in rapid drawdown with time. This model may be pessimistic due to the fact that only the net production is considered in the study. Loss of reinjected fluid to former discharge zones of the reservoir would soften this conclusion drastically. Also not considered is the possible expansion of boiling zones in the reservoir which will reduce drawdown rates.

5. A 3-D natural state model was developed. It simulates reasonably well the temperature distribution in the Miravalles wellfield. The model needs, however, the large recharge rate of 180 kg/s of 270°C fluid and exceptionally low thermal conductivity of model boundaries (0.08 W/m/°C) in order to match the field data. The main help for this might be to shorten the distance to the boundaries.

The 3-D simulation provides valuable insight into the complications that might arise in distributed parameter modelling. This has in particular to do with the model boundaries, sinks and sources. What, for example, is the nature of the upflow zone underneath the Miravalles volcano. Is it possible that a steam zone is recharging the lateral flow zone with 245°C fluid? It is also possible that due to an unknown separation mechanism under the volcano, some very acid fluid is being recharged into the wellfield, encountered in wells PGM-02 and PGM-19. The nature of the discharge zone in the south is also of interest. Given that reinjection fluid is lost to this volume at present, what will happen when the wellfield pressure falls below the discharge zone pressure?

Questions of this type must be addressed in future modelling work in Miravalles. This requires the long time work of several people and critical selection of the model properties. Other factors such as additional pressure monitoring wells and analysis of tracer test data may also help in future reservoir performance studies.

ACKNOWLEDGEMENTS

I would like to thank Dr. Ingvar B. Fridleifsson, director of the UNU Geothermal Training Programme, for giving me the opportunity to improve my knowledge. His very successfully effort in the guidance

of this programme is reflected in its high level. I also want to extend thanks to Lúdvík S. Georgsson and Gudrún Bjarnadóttir for their assistance given during the course. Also to all the lecturers and staff members at Orkustofnun for sharing their knowledge with us and their help. Very special thanks to my advisor, Grímur Björnsson, for his excellent and unselfish guidance during all the stages of this report, and for his continuous effort in providing me with the knowledge in my specialization. His contributions were invaluable for this report. I am grateful to my UNU fellow Rosanna A. Requejo, who in spite of her busy schedule with her own report, helped me alot with the translation of the geology part.

Back home, I want to express my gratitude to the people in Instituto Costarricense de Electricidad for giving me the opportunity to attend this course and helping me during this time: Dr. Alfredo Mainieri, head of the Geothermal Resourses Department and Antonio Yock, head of the Geothermal Development Office; Jorge A. Acuña, former head of the Geothermal Development Office; my partners Carlos González, Carlos Villarreal and Dagoberto Herrera for providing me with the information I used. My special thanks to my wife, parents and whole family for their spiritual and never-ending loving support.

REFERENCES

Arason, P., and Björnsson, G., 1994: *ICEBOX.* 2nd edition, Orkustofnun, Reykjavík 38 pp.

Axelsson, G., 1989: Simulation of pressure response data from geothermal reservoirs by lumped parameter models. *Proceedings of the 14th Workshop on Geothermal Reservoir Engineering, Stanford University, California,* 257-263.

Axelsson, G., 1996: *Simple modelling of geothermal systems.* UNU G.T.P., unpublished lecture notes.

Axelsson, G., and Arason, P., 1992: *LUMPFIT, automated simulation of pressure changes in hydrological reservoirs. Version 3.1, user's guide.* Orkustofnun, Reykjavík, 32 pp.

Haukwa, C., Bödvarsson, G.S., Lippmann, M.J., and Mainieri, A., 1992: Preliminary reservoir engineering studies of the Miravalles geothermal field, Costa Rica. *Proceedings of the 17th Workshop on Geothermal Reservoir Engineering. Stanford University, California,* 127-137.

Helgason, P., 1993: *Step by step guide to BERGHITI. User's guide.* Orkustofnun, Reykjavík, 17 pp.

Herrera, D., 1994: *Update of the geology conceptual model.* Miravalles Geothermal Power Project 15th Advisory Panel Meeting, Instituto Costarricense de Electricidad, Departamento Recurso Geotérmico.

ICE/ELC, 1995: *Proyecto geotérmico Miravalles: Informe de factibilidad 3a. y 4a. unidad.* Instituto Costarricense de Electricidad and ELC Electroconsult, San José, report GMV-2-ELC-R-12400(R01).

Pruess, K., 1987: *TOUGH user's guide.* Lawrence Berkeley Laboratory, University of California, report LBL-20700, 78 pp.

Quijano C., J.E., 1994: A revised conceptual model and analysis of production data for the Ahuachapán-Chipilapa geothermal field in El Salvador. Report 10 in: *Geothermal Training in Iceland 1994.* UNU G.T.P., Iceland, 237-266.

APPENDIX: Temperature and pressure cross-sections for Miravalles at selected depths

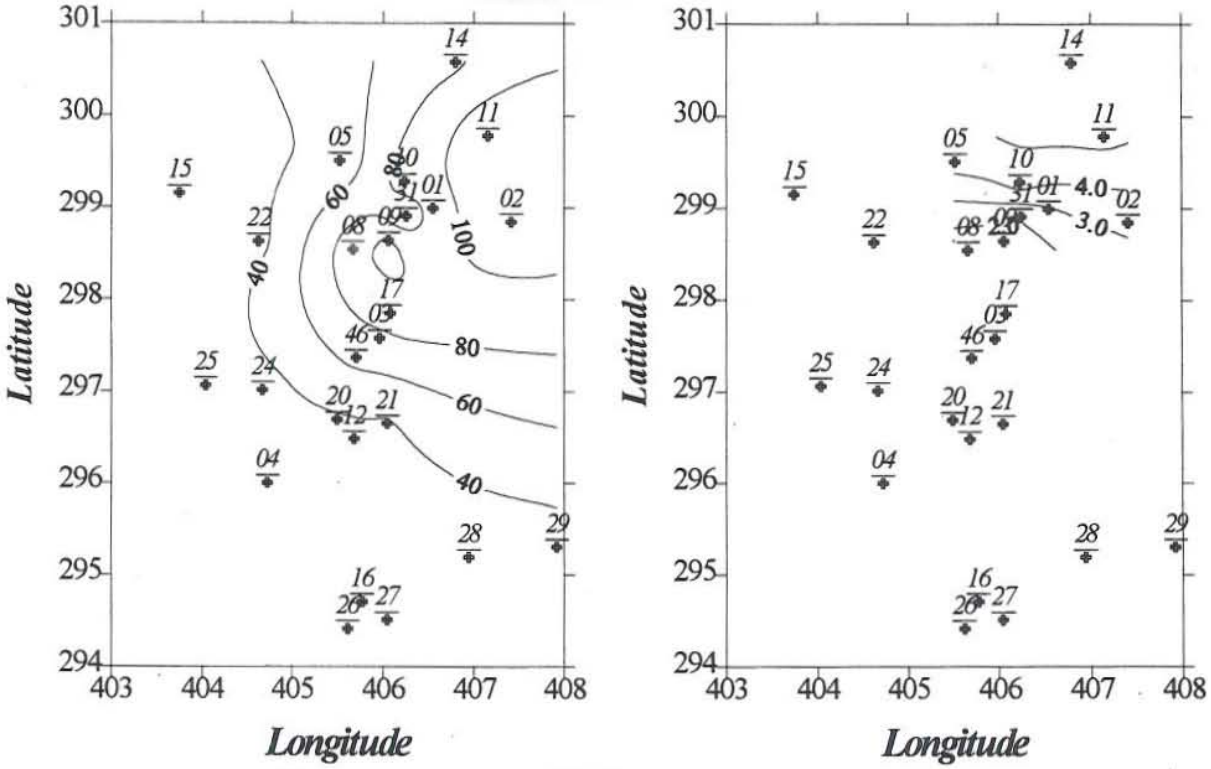

Temperature and pressure cross-sections at 400 m a.s.l.

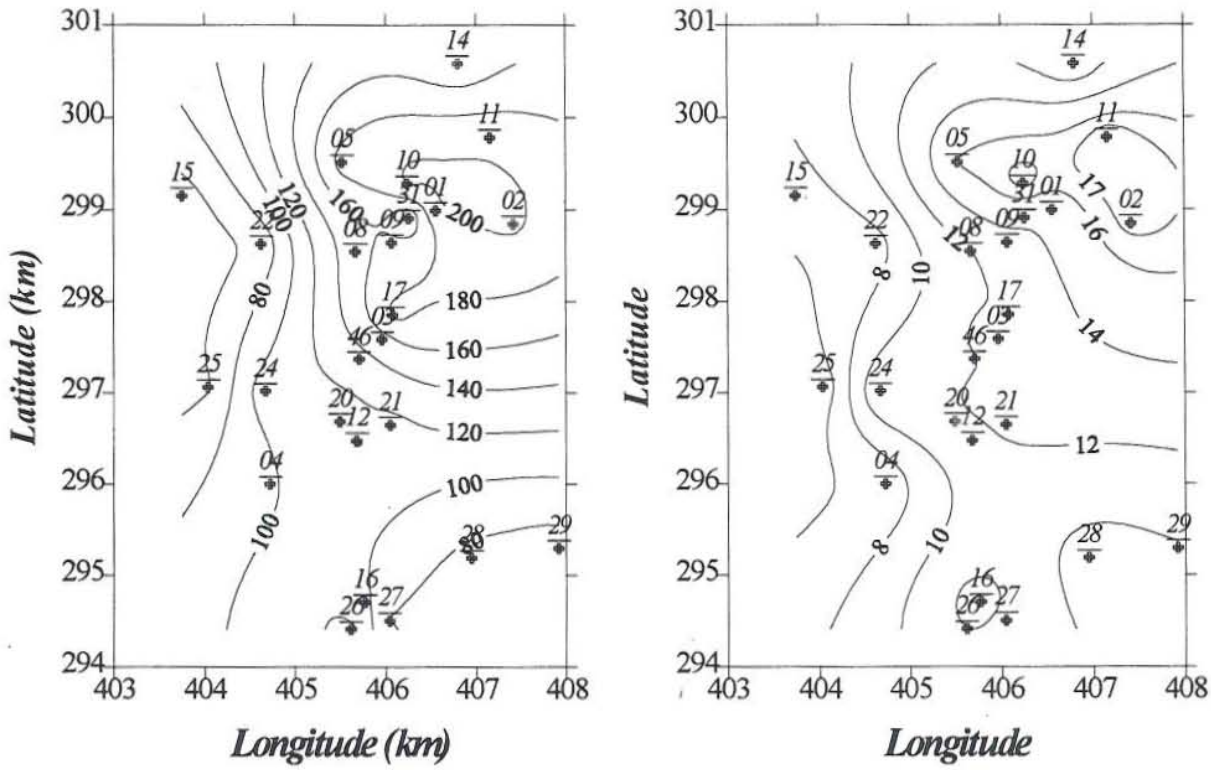

Temperature and pressure cross-sections at 200 m a.s.l.

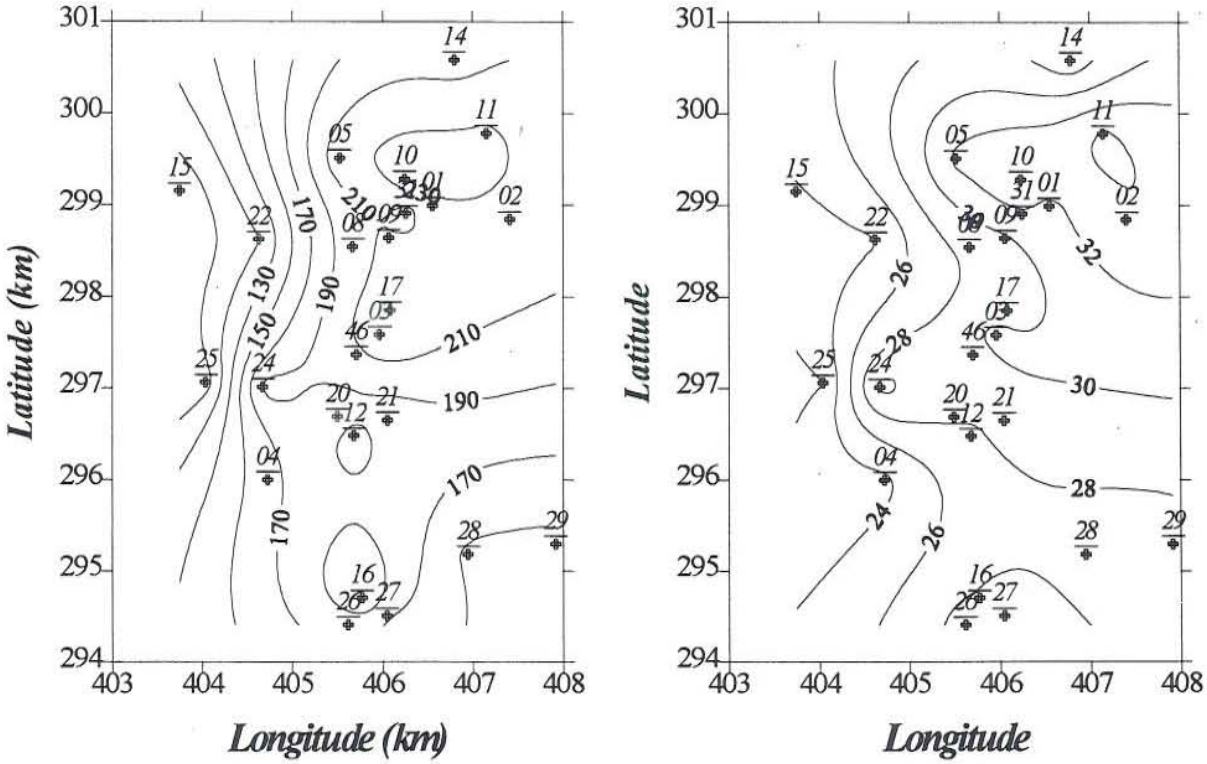

Temperature and pressure cross-sections at sea level

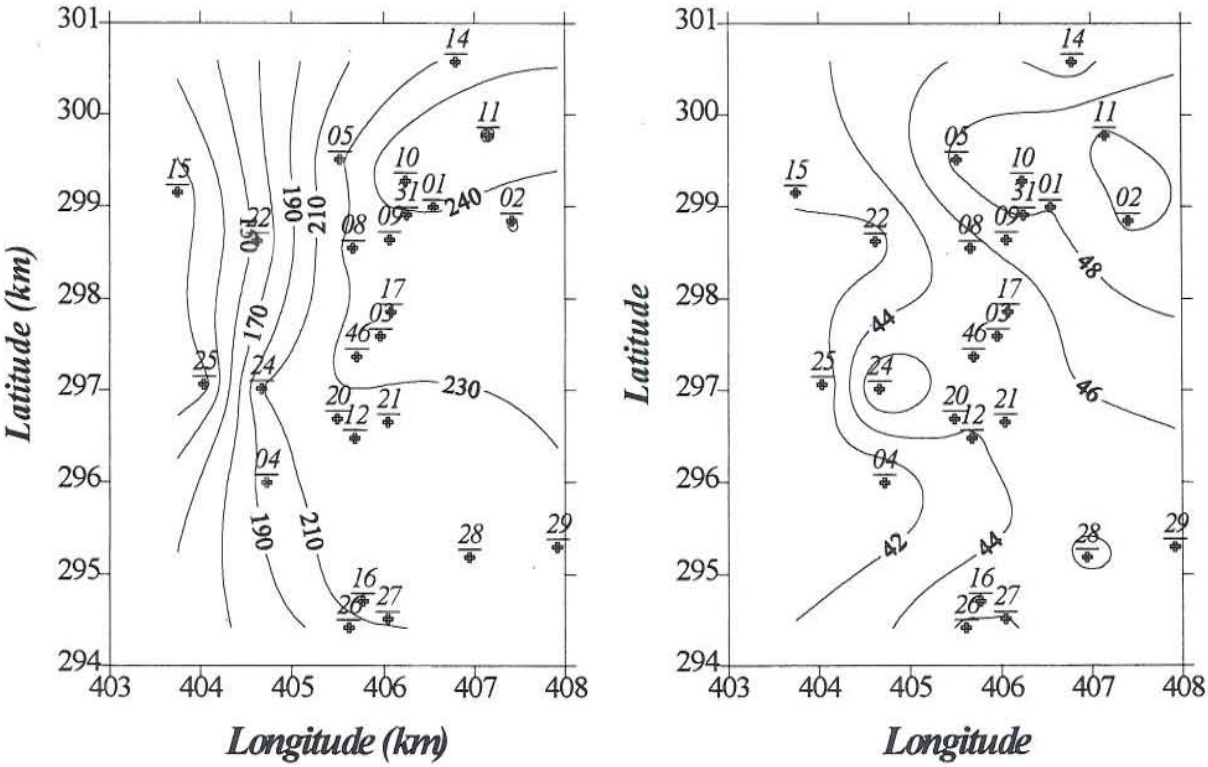

Temperature and pressure cross-sections at -200 m a.s.l.

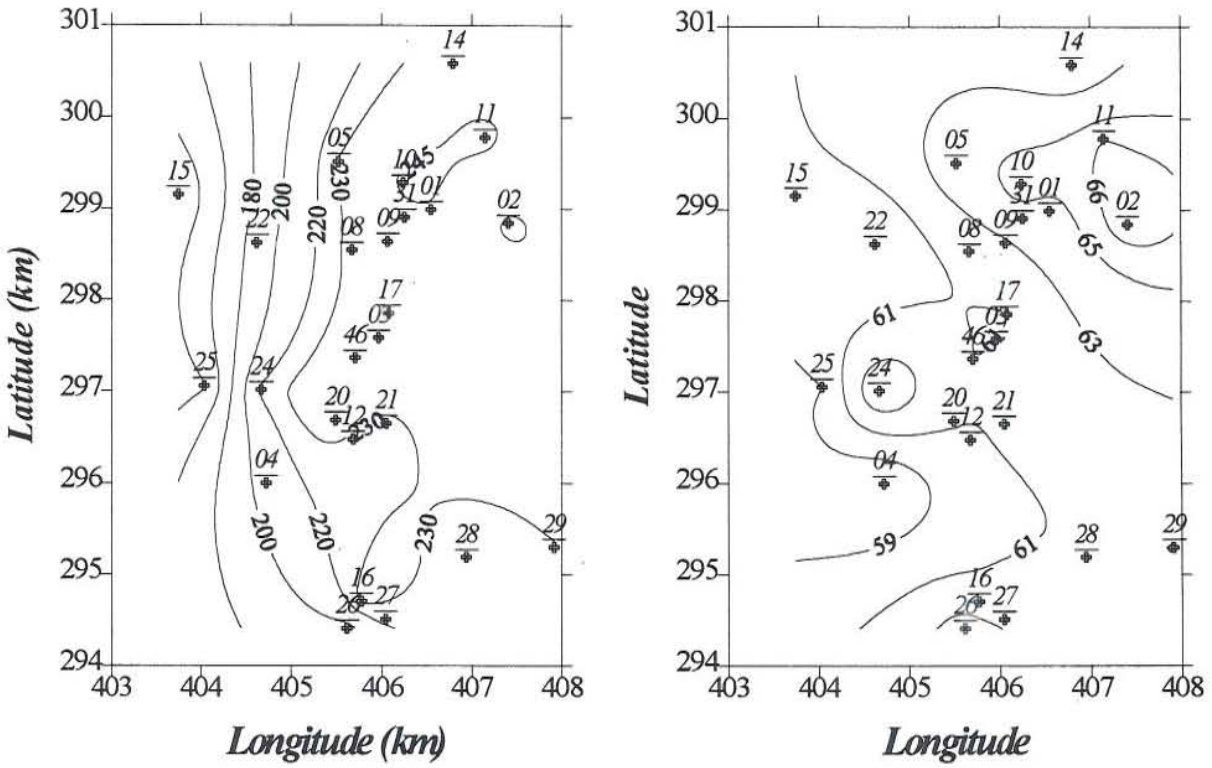

Temperature and pressure cross-sections at -400 m a.s.l.

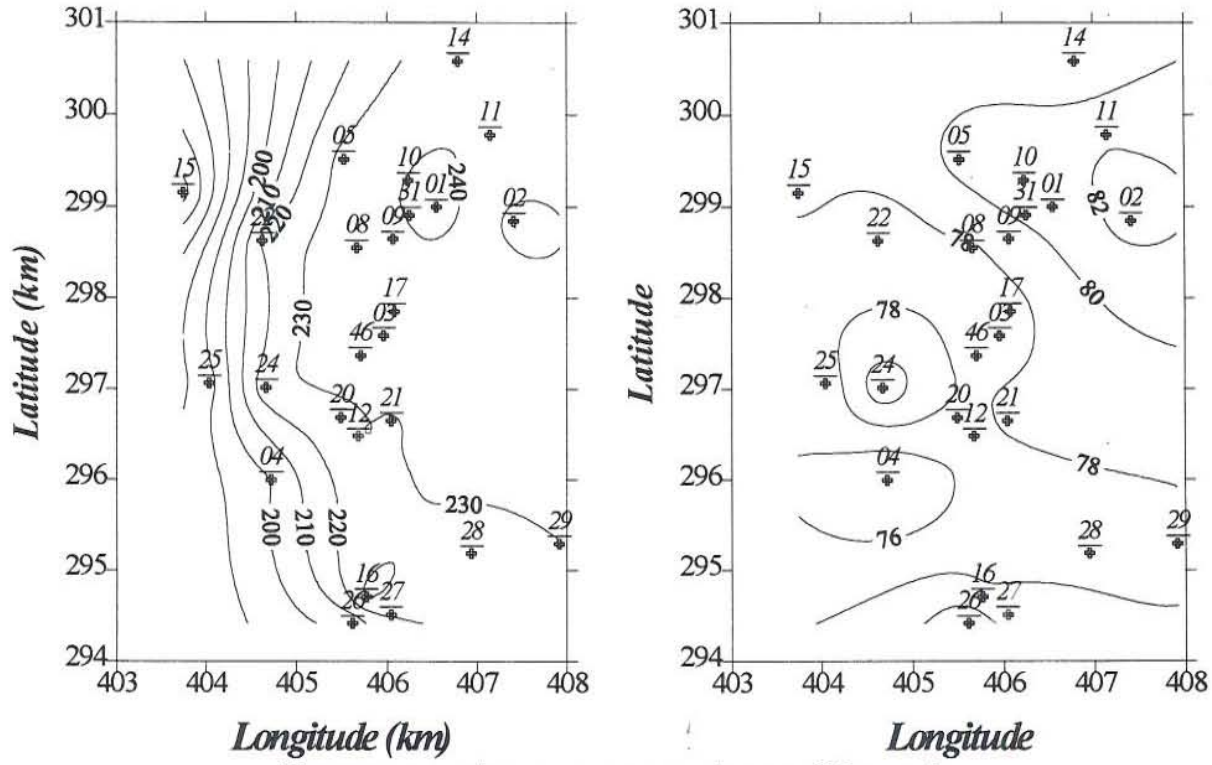

Temperature and pressure cross-sections at -600 m a.s.l.

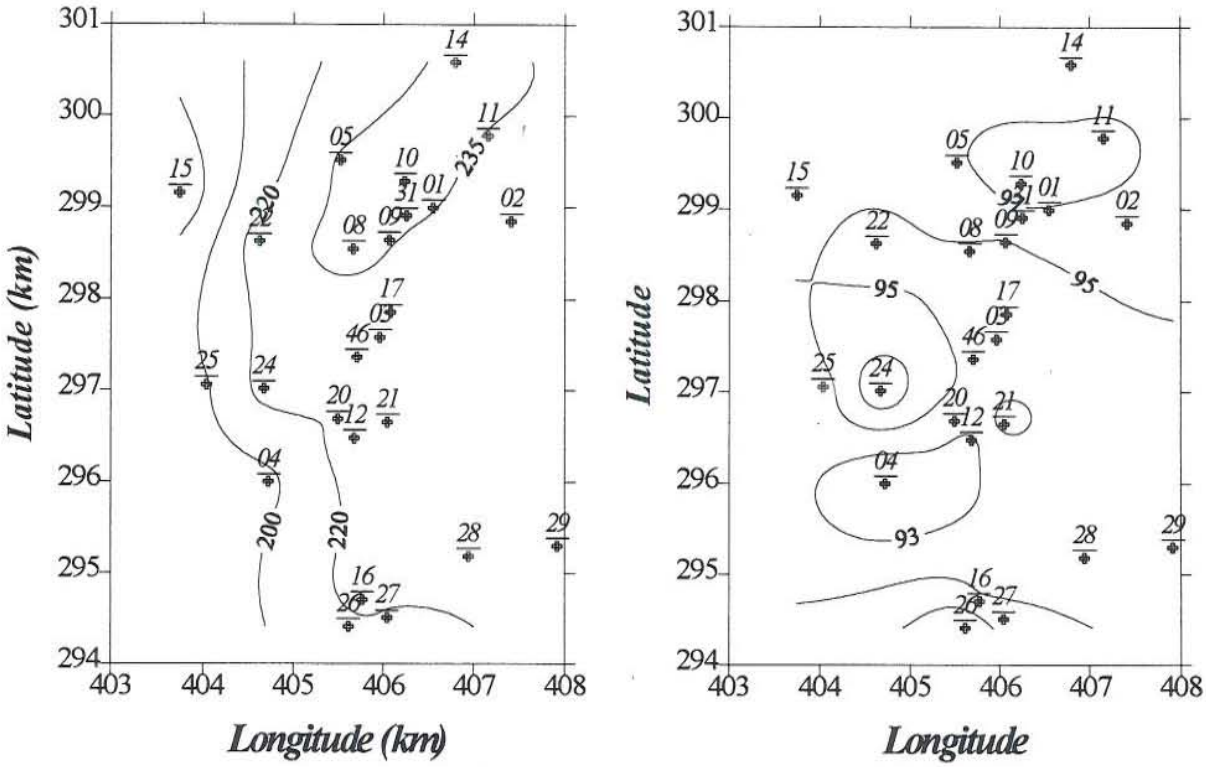

Temperature and pressure cross-sections at -800 m a.s.l.

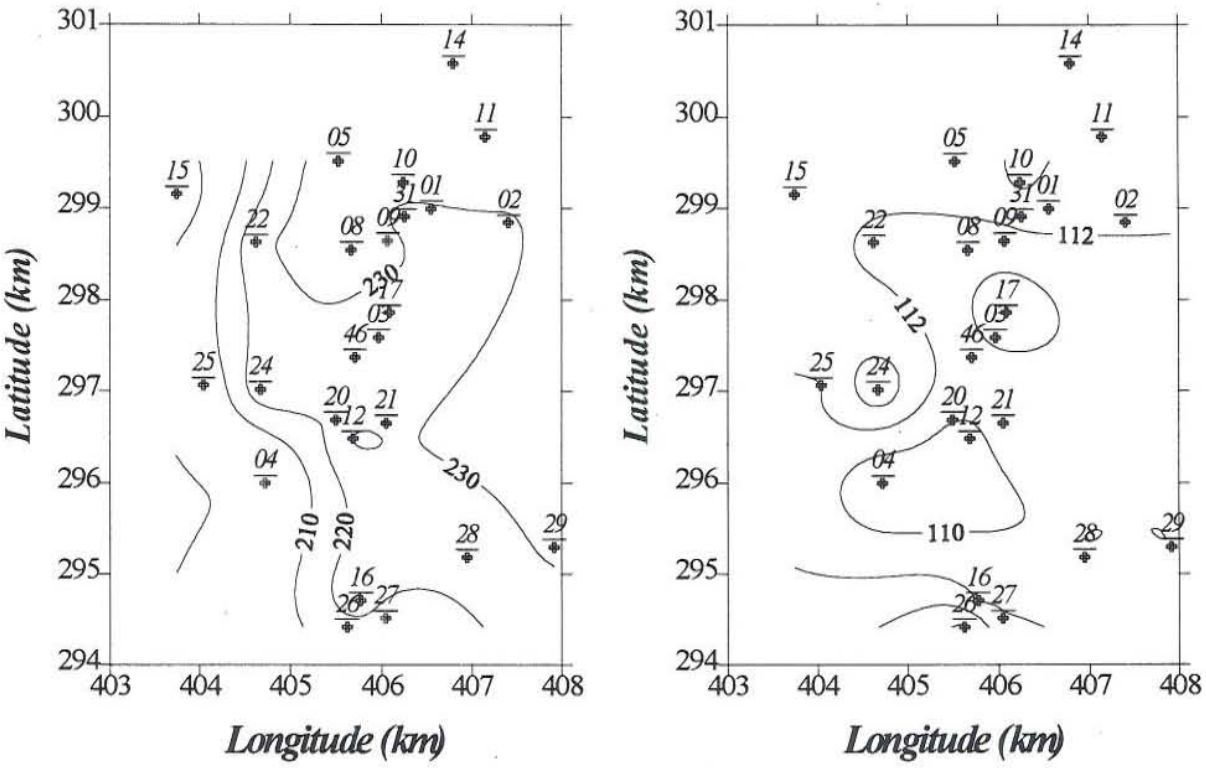

Temperature and pressure cross-sections at -1000 m a.s.l.